Influence of activation conditions on textural properties and performance of activated biochars for pyrolysis vapors upgrading

Christian Di Stasi[1*], *Gianluca Greco*[1], *Rafael L. S. Canevesi*[2], *M. Teresa Izquierdo*[3], *Vanessa Fierro*[2], *Alain Celzard*[2], *Belén González*[1], *Joan J. Manyà*[1]

[1] Aragón Institute of Engineering Research (I3A), Technological College of Huesca, University of Zaragoza, crta. Cuarte s/n, Huesca, E-22071, Spain

[2] Université de Lorraine, CNRS, IJL, Épinal, F-88000, France

[3] Instituto de Carboquímica (ICB-CSIC), Miguel Luesma Castán 4, Zaragoza, E-50018, Spain

[*] Corresponding author at: *Aragón Institute of Engineering Research (I3A), Technological College of Huesca, University of Zaragoza, crta. Cuarte s/n, Huesca, E-22071, Spain.*

E-mail address: christiandistasi@unizar.es.

ABSTRACT

The main aim of the present study is to provide a comprehensive assessment of the effects of process activation conditions on the textural properties of the resulting activated carbons, which were produced from wheat straw-derived biochar through chemical activation (with K_2CO_3 at different pressures and mass impregnation ratios) and physical activation (with CO_2 at different temperatures and pressures). For chemically activated biochars, it was found that specific surface area and pore size distribution were both only positively affected by increasing the carbonate loading. However, physically activated biochars produced at the highest pressure and lowest temperature (1.0 MPa and 700 °C) had the highest surface areas and widest pore size distributions. The materials with the most appropriate textural properties were then tested as catalysts for steam and dry reforming of the aqueous phase of pyrolysis oil. The best catalytic performance (a total gas yield of 74% and a selectivity toward H_2 of almost 40%) was observed for a physically activated biochar. This good performance was ascribed to the high availability of K^0 on the catalyst surface, which could effectively promote the reactions involved in the upgrading process.

Keywords

Biochar; chemical activation; K_2CO_3; physical activation; pressure; steam and dry reforming of pyrolysis oil

1. Introduction

In recent years, the demand for activated carbons has increased due to their usefulness in a wide range of different applications such as gas and liquid purification [1], electrochemistry [2], soil remediation [3] and catalysis [4]. Thanks to their versatility to be adapted to specific applications, these materials are considered promising candidates to address environmental issues related to global warming and pollution [5]. Nevertheless, the current main drawback is that the production of activated carbons is still partly based on fossil fuels, which do not meet sustainability criteria [6,7]. Hence, much more efforts should be made to produce much more carbons from biomass. However, the direct conversion of biomass feedstock into the final product has a low yield. Thus, the production of activated carbons from biochar produced by slow pyrolysis seems to be more appropriate in terms of scalability, while at the same time these value-added materials can strengthen the value chain of existing biochar production systems.

In general, pristine biochar has neither a well-developed surface area nor a hierarchical pore size distribution, which is mainly dominated by narrow pores with a diameter (d_p) lower than 0.7 nm (ultra-micropores). Hence, a subsequent activation step is required to improve the textural properties of the carbon material. The activation process involves the development and opening of the porosity of a char using an activation agent. Depending on the agent used, the procedure can be called chemical or physical activation. Chemical activation usually involves two steps. First, the biochar is impregnated with an aqueous solution of the chemical activation agent, or mixed with it in the dry state, and, in a second step, the blend is heated up to a given temperature at which oxidation, dehydration, aromatization and crosslinking reactions, among others, occur. Although the most widely used chemical reagents are KOH [8] and H_3PO_4 [9], non-hazardous and relatively cheap alternative compounds such as K_2CO_3 [10,11] have recently attracted considerable attention. Mai *et al.* [12] have recently reported that activation

with potassium carbonate can result in carbons with a high percentage of structural defects and a well-balanced porosity between micro- and mesopores.

When activation is carried out by exposing the precursor to relatively high temperatures under an oxidizing atmosphere (e.g., CO_2 [13], H_2O [14] and O_2 [15]), the process is called physical activation. Through either physical or chemical activation, it is possible to tune the textural features of the starting biochar by properly adjusting the activation conditions, mainly temperature, type and/or concentration of activation agent, as well as pressure. To the best of our knowledge, although both activation procedures are widely reported in the literature, a thorough study on the effects that the activation parameters and their possible interactions have on the textural properties of the resulting activated biochar, has never been reported so far. Such information could be very helpful to properly establish the most appropriate operating conditions to produce engineered carbon materials from biomass.

One of the most interesting fields of application of activated carbons is the upgrading of raw pyrolysis vapors, which contain both permanent gases (e.g., CO_2, CO, CH_4, and H_2) and condensable compounds. The condensable fraction, which is generally called pyrolysis oil or bio-oil, is a mixture of hundreds of organic compounds (alcohols, ketones, acids, etc.) and water, and its composition strictly depends on the biomass composition and the pyrolysis operating conditions [16]. For biochar production systems based on slow pyrolysis, downstream processes aimed at upgrading pyrolysis vapors are required to avoid undesirable condensation of organic compounds and to increase simultaneously the quality of the gaseous product. For this purpose, combined steam and dry reforming of pyrolysis oil is a promising option [17,18], due to the presence of a relatively high amount of CO_2 and steam in the raw vapor phase. Heterogeneous catalysts based on transition metals such as Ni [19,20], Co [21], Pt and Rh [22] can be used to improve the overall conversion and the selectivity of the products. However, the main drawback of these catalysts is that the relatively expensive active phase can

easily be poisoned and/or deactivated by deposition of coke [23]. One possible solution to reduce the overall cost of the upgrading process is to use activated biochar as catalyst. Its porous structure and inherent inorganic contents (especially K, Mg and Ca) could result in a relatively good catalytic activity [24–29]. Furthermore, due to the presence in the reaction system of H_2O and CO_2, the carbonaceous support, as well as coke deposits, could be continuously partly gasified, thus creating new pores to avoid deactivation. In addition, the spent biochar can be burned to recover energy [30] or, depending on the metal loaded on the support, employed as soil conditioner [31].

Keeping in mind all the above, the main objective of this study was to perform a preliminary investigation about the effects of several activation conditions on the textural properties and the catalytic activity of the resulting activated biochars. To this end, wheat straw-derived biochar was activated chemically and physically with K_2CO_3 and CO_2, respectively, under different operating conditions. To objectively assess the effect of the selected operation conditions (temperature and mass ratio K_2CO_3/precursor for chemical activation, and temperature and pressure for CO_2 activation), we implemented two factorial designs of experiments, with two factors and three replicates at the center point. The specific surface areas and pore size distributions of the resulting activated biochars were then evaluated. The most promising activated biochars were finally tested as catalysts for steam and dry reforming of pyrolysis oil. Their performance was evaluated in terms of conversion of liquid into gas, product selectivity and resistance to deactivation.

2. Experimental Section

This study was divided into two main steps: in the first, we carried out physical and chemical activations under different process conditions in order to study their influence on the pore size distribution and specific surface area of the resulting activated biochars; in the second part, the most promising materials were then tested as catalysts in pyrolysis vapors

upgrading experiments. The methodology used in this study is summarized graphically in Fig. A.1.

2.1. Biochar production

The biochar used in this study was produced by slow pyrolysis of binder-free wheat straw pellets (9 mm OD and 10–13 mm long). Pyrolysis was carried out at atmospheric pressure in a fixed bed reactor, which was placed inside a furnace and heated up to 500 °C at an average heating rate of 5 °C min^{-1} and using N_2 as carrier gas. More details on the pyrolysis device and the experimental procedure are available elsewhere [32]. The resulting biochar (i.e., "pristine") was ground and then thoroughly sieved to obtain particle sizes in the range of 0.212 to 1.41 mm. The pristine biochar was characterized by proximate analysis (performed in quadruplicate according to ASTM standards D3173 for moisture, D3174 for ash, and D3175 for volatile matter) and ultimate analysis by means of an elemental analyzer CHN628 from Leco Corporation (USA).

2.2. Activation of pristine biochar

2.2.1. Chemical activation

For chemical activation, the pristine biochar was first impregnated with a 1 mol L^{-1} aqueous solution of K_2CO_3. Three K_2CO_3: biochar mass impregnation ratios (1:1, 2:1 and 3:1) were achieved by adjusting the volume of solution. The heterogeneous mixture was then stirred for 2 h at 50 °C, filtered and dried overnight at 110 °C to remove the residual water. Afterwards, 10 g of the impregnated samples were heated up to 700 °C at a heating rate of 10 °C min^{-1}, under an inert atmosphere (N_2), and at three different values of absolute pressure (0.10, 0.55 and 1.00 MPa). For this purpose, a tubular fixed bed reactor (made of nickel-chromium alloy UNS N06600, 28.1 mm ID and 600 mm long) placed in a vertical furnace (model EVA 12/300 from Carbolite Gero, UK) was used. The relatively low activation temperature was chosen to avoid the evaporation of the metallic potassium derived from the decomposition of the

activation agent and, also, to ensure low activation extensions and clearly see the potential effects of the studied parameters. On the other hand, the range of activating pressures was chosen in order to allow this experimental setup to be easily scaled up, since the involved pressures were not too high (up to 1.0 MPa). A soaking time at the highest temperature of 60 min was set. The pressure within the reactor was adjusted using a downstream servo-controlled regulator valve. The gas hourly space velocity (GHSV) at the activation temperature was estimated to be 7000 h^{-1}, considering the pressure applied and a bed void factor of 0.5. Thus, the mass flow rate of the inlet gas stream (N_2) was properly adjusted as a function of the selected pressure and the highest temperature to achieve the aforementioned GHSV value.

As a last step, the carbons were rinsed to remove the unreacted reagent and other impurities from their surface. In this work, two different washing procedures were adopted to assess possible effects on the resulting surface area and the catalytic activity of the activated carbons produced. For this purpose, among all the unwashed chemically activated biochars, four of them were just washed with hot deionized water (100 °C), while the seven chemically activated biochars adopted in the design of experiments were washed with a 0.25 mol L^{-1} solution of HCl followed by hot water. Both washing procedures were carried out until neutral pH. The resulting activated biochars were then dried overnight at 110 °C. The efficiency of the washing step was evaluated according to the washing yield, calculated from Eq. 1, in which m_c and m_w are the masses of activated carbon before and after the washing steps, respectively.

$$Y_{wash} = \left(1 - \frac{m_c - m_w}{m_c}\right) 100 \quad (1)$$

2.2.2. Physical activation

Physically activated biochars were produced under an atmosphere of pure CO_2 at three different temperatures(700, 775 and 850 °C), and at three different absolute pressures (0.10, 0.55, and 1.00 MPa). The selected activation temperatures are within the range commonly reported in the literature, whereas the pressure values were established with the purpose to

compare the properties of resulting activated carbons produced under atmospheric and moderate pressures. Using the same device described in the previous section, 10 g of pristine biochar were heated under N_2 atmosphere, at a heating rate of 10 °C min^{-1}, until the target temperature was reached. Then, the gas supply was switched from N_2 to CO_2 at a constant GHSV of 7000 h^{-1}. These conditions were maintained during the time required to reach a degree of burnout (η, defined as the percentage of mass loss) in the range of 30% to 60%.

2.2.3. Design of experiments

To objectively assess the effects of the activation conditions on the textural properties of activated biochars, an unreplicated two-level factorial design of experiments (with two factors and three replicates at the center point) was adopted for both chemical and physical activations. For chemical activation, the analyzed factors were the absolute pressure and the impregnation ratio of K_2CO_3 to raw biochar, whereas in the case of physical activation, the temperature and the absolute pressure were the studied factors. The structure of the regression model used in the statistical analysis was the following:

$$\hat{y} = \beta_0 + \beta_i A + \beta_j B + \beta_{ij} AB \quad (2)$$

where *A* and *B* corresponded to the assessed factors (normalized values in the range from –1 to 1), whereas β_0, β_i, and β_{ij} were the intercept, linear, and interaction coefficients, respectively. The results obtained for the selected response variables (*y*) were analyzed using the Minitab v17 statistical package. A significance level of 5% was assumed and the adjusted coefficient of determination (R^2_{adj}) was taken as an indicator of the quality of the fit. Table 1 summarizes the adopted designs of experiments and lists the names of the activated biochars produced. Briefly, activated biochar are referred as *X_Y_P*. *X* corresponds to the activation procedure (CB or PB for *chemically activated biochar* and *physically activated biochar*, respectively); *Y* is the activation temperature for PBs or the impregnation ratio for CBs; and *P* is the activation pressure.

2.3. Catalytic pyrolysis vapors upgrading

The liquid feed used here for pyrolysis vapors upgrading tests was the filtered aqueous phase of the pyrolysis oil formed during the production of pristine biochar derived from wheat straw. This resulting liquid product was characterized in terms of elemental composition, using the same CHN analyzer as mentioned in section 2.1, and water content, using a volumetric Karl-Fischer titrator Titrino plus 870 from Metrohm (Switzerland).

A schematic overview of the experimental device used for the reforming tests is shown in Fig. A.2 (Appendix A). The reactor and furnace elements were the same as those previously described in section 2.2. The reforming operating conditions were selected based on the findings of a previous study [33], which aimed to establish the best process conditions to minimize deactivation by coke deposition.

Briefly, activated biochar (2–5 g) was loaded into the reactor and heated under N_2 atmosphere at an absolute pressure slightly above 0.1 MPa. Once the bed temperature reached the target value of 750 °C, CO_2 was added to the inlet gas stream at a partial CO_2 pressure of 0.02 MPa. The liquid feed was then injected into the gas stream at the inlet of the reactor by means of a HPLC pump (model 521 from Analytical Scientific Instruments, USA). The liquid hourly space velocity (LHSV) was kept constant and equal to 2 h^{-1} for all the experiments conducted. The duration of the experiments was 60 min. The reactor outlet stream, consisting of permanent gases, unreacted pyrolysis oil, and condensable side products, was forced to pass through an ice-bath condensation train. The permanent gases were analyzed using a dual-channel micro gas chromatograph (μ-GC 490 from Agilent, USA) equipped with TCD detectors and two analytical columns (a Molsieve 5 A and a PolarPlot U). The known amount of N_2 fed was used as a tracking compound to calculate the yield of produced gas.

Table 1. Matrix of the factorial designs adopted to assess the effects of the selected factors during both chemical and physical activations. For example, a physical activation carried out at A=–1 and B=1 means that the process was performed at 700°C and 1.0 MPa

Chemical activation (thermal treatment under N_2 up to 700 °C and 1 h soaking time)			
	Factors		***Response Variables***
	A	*B*	$S_{2D\text{-}NLDFT}$, V_t, V_{ultra}, V_{micro}, V_{meso}
Level	Pressure (MPa)	Mass ratio (K_2CO_3: raw biochar)	
Low (–1)	0.10	1:1	
Middle (0)	0.55	2:1	
High (+1)	1.00	3:1	
Runs			**Activated biochar designation** (all washed with an acidic solution)
1	0	0	CB_2_0.55
2	–1	+1	CB_3_0.10
3	+1	+1	CB_3_1.00
4	0	0	CB_2_0.55
5	0	0	CB_2_0.55
6	–1	–1	CB_1_0.10
7	+1	–1	CB_1_1.00
Physical activation			
	Factors		***Response Variables***
	A	*B*	$S_{2D\text{-}NLDFT}$, V_t, V_{ultra}, V_{micro}, V_{meso}
Level	Temperature (°C)	Pressure (MPa)	
Low (–1)	700	0.10	
Middle (0)	775	0.55	
High (+1)	850	1.00	
Runs			**Activated biochar designation**
1	–1	–1	PB_700_0.10
2	–1	+1	PB_700_1.00
3	+1	+1	PB_850_1.00
4	0	0	PB_775_0.55
5	0	0	PB_775_0.55
6	+1	–1	PB_850_0.10
7	0	0	PB_775_0.55

The performance of the activated biochars tested was measured in terms of total gas yield (Y_g) and hydrogen yield (Y_{H2}), as defined by Eqs. (3) and (4), respectively.

$$Y_g = \frac{m_g}{m_L} 100 \quad (3)$$

$$Y_{H2} = \frac{F_{H2\,av}}{F_{H2stoi}} 100 \quad (4)$$

$$F_{H2stoi} = \left(2n + \frac{m}{2} - k\right) F_{BO} \quad (5)$$

$$S_i = \frac{n_i}{n_{tot}} 100 \quad (6)$$

In Eq. (3), m_g was the cumulative mass of the gas produced during the 60-min experiments, whereas m_L corresponded to the total mass of the liquid fed. In Eq. (4), F_{H2av} was the experimental average molar flow rate of hydrogen from minute 20 to minute 40. F_{H2stoi}, which was calculated according to Eq. (5), corresponded to the stoichiometric molar flow rate of hydrogen considering the contribution from steam reforming reaction. F_{BO} was the molar flow rate of the dry pyrolysis oil fed. The selectivity towards specific gaseous products (S_i) was calculated according to Eq. (6), in which n_{tot} was the sum of the gaseous products in moles at the outlet stream.

2.4. Characterization of carbon materials

The textural properties of pristine and activated biochars were determined from both N_2 and CO_2 adsorption isotherms at –196 °C and 0 °C, respectively. Around 120 mg of sample were degassed under vacuum at 150 °C. ASAP 2020 and ASAP 2420 automatic adsorption analyzers (Micromeritics, USA) were used. The results obtained from the isotherms were treated using the MicroActive software. We determined the BET area (A_{BET}) by application of the BET model, as well as the Gurvitch volume ($V_{0.97}$). The enhanced 2D-NLDFT model [34] was employed using SAIEUS software (available at www.nldft.com) to evaluate the pore size distributions (PSDs) and other related parameters: surface area ($S_{2D\text{-}NLDFT}$), ultra-micropore

volume (V_{ultra}, d_p < 0.7 nm), micropore volume (V_{micro}, d_p < 2 nm), total pore volume (V_t) and mesopore volume (V_{meso}, d_p in the range of 2 to 50 nm). The latter was calculated as the difference between V_t and V_{micro}.

To evaluate the availability of residual potassium carbonate on the surface of chemically activated biochars, Fourier-transform Infrared Spectroscopy (FTIR) analyses were conducted using a Frontier MIR/NIR Spectrometer from PerkinElmer (USA).

Qualitative temperature-programmed desorption (TPD) analyses of pristine biochar and fresh catalysts used in reforming tests were also performed to assess the thermal stability of these samples. TPD measurements were carried out using a thermogravimetric analyzer coupled with a mass spectrometer (STA 449 F3 and QMS 403 Aëolos Quadro from Netzsch, Germany), by heating the sample up to 750 °C at a heating rate of 5 °C min^{-1} under an Ar atmosphere.

A FEI XL30 SFEG scanning electron microscope coupled with energy-dispersive X-ray spectroscopy (Oxford Instrument EDS SDD XMAX detector) was used to characterize the surface of fresh and spent activated biochars. The secondary electron images were taken with an acceleration voltage of 3 or 5 kV to investigate the topology of the samples surface, while an acceleration tension of 10 kV was applied to carry out the chemical mapping of the materials by EDX analysis. Additionally, X-ray photoelectron spectroscopy (XPS) data of spent and fresh catalysts were recorded using an ESCAPlus OMICROM system equipped with a hemispherical electron energy analyzer, following the procedure detailed elsewhere [35].

3. Results and discussion

The results of the textural characterization as well as the proximate and ultimate analyses of the pristine biochar are summarized in Table A.1. The reported values of A_{BET} and $S_{2D\text{-}NLDFT}$ confirm that the porosity of the pristine biochar, as previously stated, was characterized by a very high fraction of ultra-micropores.

3.1. Chemical activation

Although the use of K_2CO_3 as catalyst in coal gasification processes has been widely reported in the literature [10–12,33], the mechanism explaining its interaction with the carbon matrix still remains unclear. The main reactions that probably occur during chemical activation of a carbonaceous material are the following:

$$K_2CO_3 \rightleftarrows K_2O + CO_2 \quad (7)$$

$$CO_2 + C \rightleftarrows 2CO \quad (8)$$

$$K_2CO_3 + 2C \rightleftarrows 2K + 3CO \quad (9)$$

$$K_2O + C \rightleftarrows 2K + CO \quad (10)$$

The increase in specific surface area could be ascribed to the CO_2 released from carbonate decomposition (Reaction 7), which can diffuse into the solid structure and subsequently react with carbon, thereby stimulating the production of CO by the reverse Boudouard reaction (Reaction 8) and creating vacancies in the solid structure [36]. Despite the fact that the decomposition of K_2CO_3 mainly occurs at temperatures above 900 °C, its contact with the carbon matrix can promote its decomposition a relatively low temperatures [37,38]. The potassium oxide resulting from the decomposition of the carbonate, or the carbonate itself, can also react with the carbon-based material through Reaction 9 and 10 towards CO and metallic potassium [39].

The assessed textural properties of chemically activated biochars are listed in Table 2. Fig. 1 shows the normalized plots of the standardized effects for the response variables considered: $S_{2D\text{-}NLDFT}$, V_t, V_{ultra}, V_{micro}, and V_{meso}. The PSDs obtained for biochars activated with different impregnation ratios and the N_2 adsorption isotherms of such samples are shown in Figs. A.3a and A.4, respectively. More detailed statistical outcomes for the results reported in the present section can be found in Table A.2.

285 **Table 2.** Results of textural characterization and washing efficiency of chemically activated

286 biochars

Material	Apparent specific surface area		Pore volumes					Washing yield
	A_{BET}	$S_{2D\text{-}NLDFT}$	$V_{0.97}$	V_t	V_{ultra}	V_{micro}	V_{meso}	Y_{wash}
	$m^2\ g^{-1}$		$cm^3\ g^{-1}$					%
CB_1_0.10	170	712	0.078	0.181	0.143	0.175	0.006 (3.19 %) [a]	77.0
CB_1_0.10_W [b]	142	700	0.068	0.180	0.135	0.169	0.011 (6.14 %) [a]	77.1
CB_1_1.00	180	761	0.081	0.195	0.149	0.188	0.007 (3.82%) [a]	76.4
CB_1_1.00_W [b]	100	700	0.049	0.168	0.144	0.160	0.008 (5.01%) [a]	78.1
CB_3_0.10	413	933	0.181	0.259	0.197	0.246	0.013 (4.96%) [a]	54.3
CB_3_0.10_W [b]	368	893	0.158	0.242	0.193	0.229	0.013 (5.35%) [a]	56.0
CB_3_1.00	337	834	0.148	0.230	0.169	0.218	0.012 (5.23%) [a]	56.9
CB_3_1.00_W [b]	316	851	0.138	0.229	0.180	0.217	0.012 (5.40%) [a]	60.6
CB_2_0.55	316	900	0.137	0.238	0.180	0.228	0.009 (3.92%) [a]	58.1
CB_2_0.55	310	872	0.136	0.233	0.177	0.222	0.011 (4.63%) [a]	54.4
CB_2_0.55	307	864	0.137	0.233	0.171	0.221	0.011 (4.86%) [a]	55.5

287 [a] Calculated as $\frac{Vmeso}{Vt}$ 100

288 [b] Carbons just washed with water that were not included in the design of experiments.

289

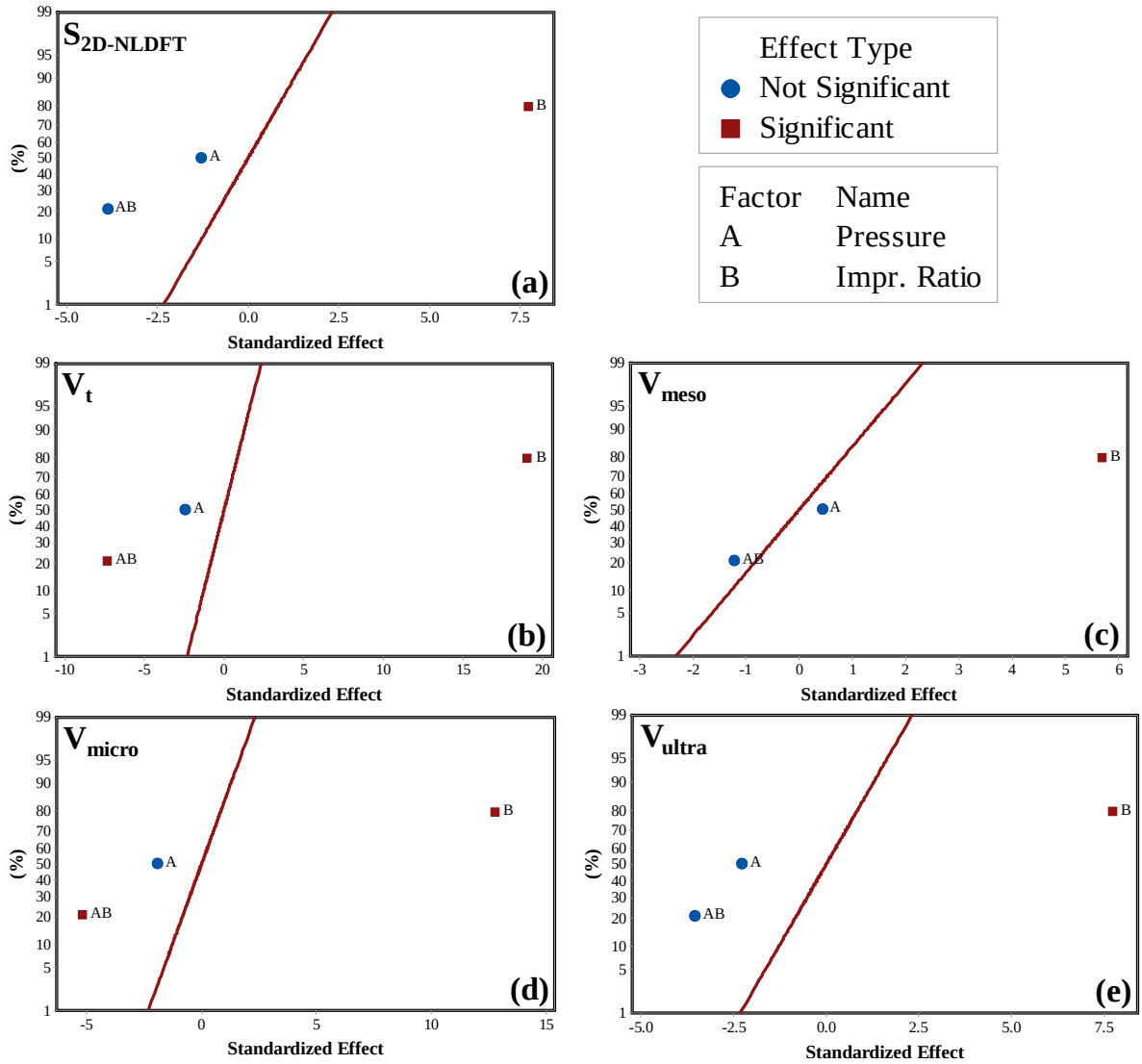

290 **Fig. 1**. Normal plots of standardized effects (α = 0.05) for chemically activated biochars:
291 specific surface area (a); total pore volume (b); mesopore volume (c); micropore volume (d);
292 ultra-micropore volume (e).

293 Regarding the results obtained in terms of specific surface area ($S_{2D\text{-}NLDFT}$), Fig. 1a clearly
294 shows that a higher concentration of activation agent led to a significant increase in the porosity
295 of the resulting activated biochars. In contrast, the absolute pressure proved to be irrelevant for
296 the values of final specific surface area. Our results regarding the development of porosity
297 when higher impregnation ratios were used confirm the relevance of K_2CO_3 as a chemical
298 reagent for the production of tailored activated carbons. All pore volumes analyzed in the

present study were also found to be strongly dependent on the amount of activating agent (see Fig. 1). The chemical activation process was able to slightly broaden the original pore size distribution of the pristine biochar, leading to a more hierarchical porous structure with a large contribution of ultra-micropores and a slightly increased amount of mesopores. Almost all the carried out N_2 isotherms required more than 70 h to be completed, thus confirming the predominant narrow microporous structure of chemically activated biochars (see Fig. A.3a), which hindered the diffusion of N_2 within the porosity. For both total and micropore volumes, a statistically significant combined effect of pressure and impregnation ratio (AB) was found. However, these effects were comparatively much weaker than that observed for the main effect of the impregnation ratio (B). From a thermodynamics point of view, an increased pressure shifts the equilibrium of the activation reactions to the left. The fact that the textural properties of the resulting activated carbons were practically independent of pressure could indicate that the chemical activation process was mainly kinetically controlled.

It should be pointed out that the overall curvature terms for $S_{2D\text{-}NLDFT}$, V_t and V_{micro} were statistically significant (*p*-values below 0.05, as reported in Table A.2). This indicates that, in further studies, our adopted factorial design should be expanded to a central composite design to be able to evaluate the pure quadratic regression coefficients and then apply Response Surface Methodology (RSM) for optimization purposes.

As shown in Table 2, after the carbons were washed only with hot water, there was a slight decrease in both the specific surface area and the micropore volume, compared to those measured for carbons washed with the acidic solution. This can be explained by the fact that water could not completely remove the remaining carbonate (and other chemical species) from the solid surface, thus causing blockage of some micropores. By focusing on the difference between the washing procedures of activated carbons at the same loadings of K_2CO_3, the results reported in Table 2 indicate that a higher activation pressure led to an increased amount of

product not soluble in water, i.e., to higher Y_{wash} values. This finding agrees with results reported by Malekshahian *et al.* [40], who concluded that high gasification pressures can limit the volatilization of potassium.

3.2. Physical activation

It must be pointed out that an increase in absolute pressure also implied an increase in the partial pressure of the reactant (CO_2). In the literature, the effects of absolute pressure and partial pressure of reactant are commonly assessed separately. Nevertheless, and as far as we know, no previous studies have addressed the question of whether activation under pressure can cause textural changes in the resulting physically activated biochars. Activation of biomass-derived carbon had only been studied using supercritical water at high pressure [41], but such conditions are too different from the present ones for allowing some comparison to be done.

Table 3 lists the textural properties of the activated carbons produced, whereas Fig. 2 shows the normal plots of the standardized effects obtained for each response variable. More detailed statistical outcomes are reported in Table A.3. The most relevant PSDs and N_2 adsorption isotherms are shown in Figs. A.3b and A.5, respectively. As previously mentioned in section 2.2.2, the activation times (also shown in Table 3) were varied to obtain degrees of burnout in the range of 30% to 60 %, since the gasification rate was strictly dependent on reaction temperature and reactant partial pressure. As expected, the reaction rate was minimal at the lowest temperature (700 °C). In fact, and whatever the pressure applied, an activation time of 180 min was required to reach the desired reaction extent. For activation temperatures of 775 and 850 °C, an activation time of 60 min was enough, except for the material PB_850_1.00, for which this reaction time led to an almost complete gasification of the sample (η = 85%). Hence, the activation time at the highest levels of temperature and pressure was finally set at 30 min to obtain a degree of burnout of 57%.

Table 3. Degrees of burnout activation times and textural properties for physically activated biochars

Material	Activation time	Burnout	Apparent specific surface area		Pore volumes				
	t_{act}	η	A_{BET}	$S_{2D\text{-}NLDFT}$	$V_{0.97}$	V_t	V_{ultra}	V_{micro}	V_{meso}
	min	%	$m^2\ g^{-1}$		$cm^3\ g^{-1}$				
PB_700_0.10	180	30.1	552	833	0.237	0.243	0.184	0.227	0.016 (6.77%) [c]
PB_700_1.00	180	52.8	743	1008	0.333	0.333	0.226	0.301	0.032 (9.55%) [c]
PB_850_0.10	60	54.9	600	818	0.263	0.266	0.169	0.240	0.026 (9.64%) [c]
PB_850_1.00	30	56. 7	688	881	0.298	0.296	0.176	0.273	0.022 (7.57%)[c]
PB_775_0.50	60	43.7	719	931	0.314	0.312	0.176	0.285	0.027 (8.62%)[c]
PB_775_0.50	60	42.2	707	936	0.309	0.306	0.171	0.282	0.025 (8.02%) [c]
PB_775_0.50	60	42.4	707	949	0.308	0.306	0.174	0.282	0.023 (7.64%) [c]
PB_650_0.10 [d]	60	12.5	68.8	482	0.029	0.126	0.100	0.124	0.001 (1.07%) [c]
PB_650_1.00 [d]	180	25.0	447	750	0.191	0.214	0.154	0.200	0.014 (6.46%) [c]

[c] Calculated as $\frac{Vmeso}{Vt}$ 100

[d] Additional carbons that were not included in the design of experiments.

It was clear that a high pressure accelerated carbon gasification, even at 700 °C. At this temperature, an increase in pressure from 0.1 to 1.0 MPa led to a marked increase in the burnout, from 30.1% to 52.8%, due to the higher reaction rate. In this sense, an increased CO_2 partial pressure resulted in a higher fraction of reactant adsorbed on the surface of the sample [42]. These outcomes are in agreement with the study conducted by Malekshahian *et al.* [42], but disagree with the results reported by Fermoso *et al.* [43], who observed that gasification of heartwood was enhanced using low partial pressures of CO_2.

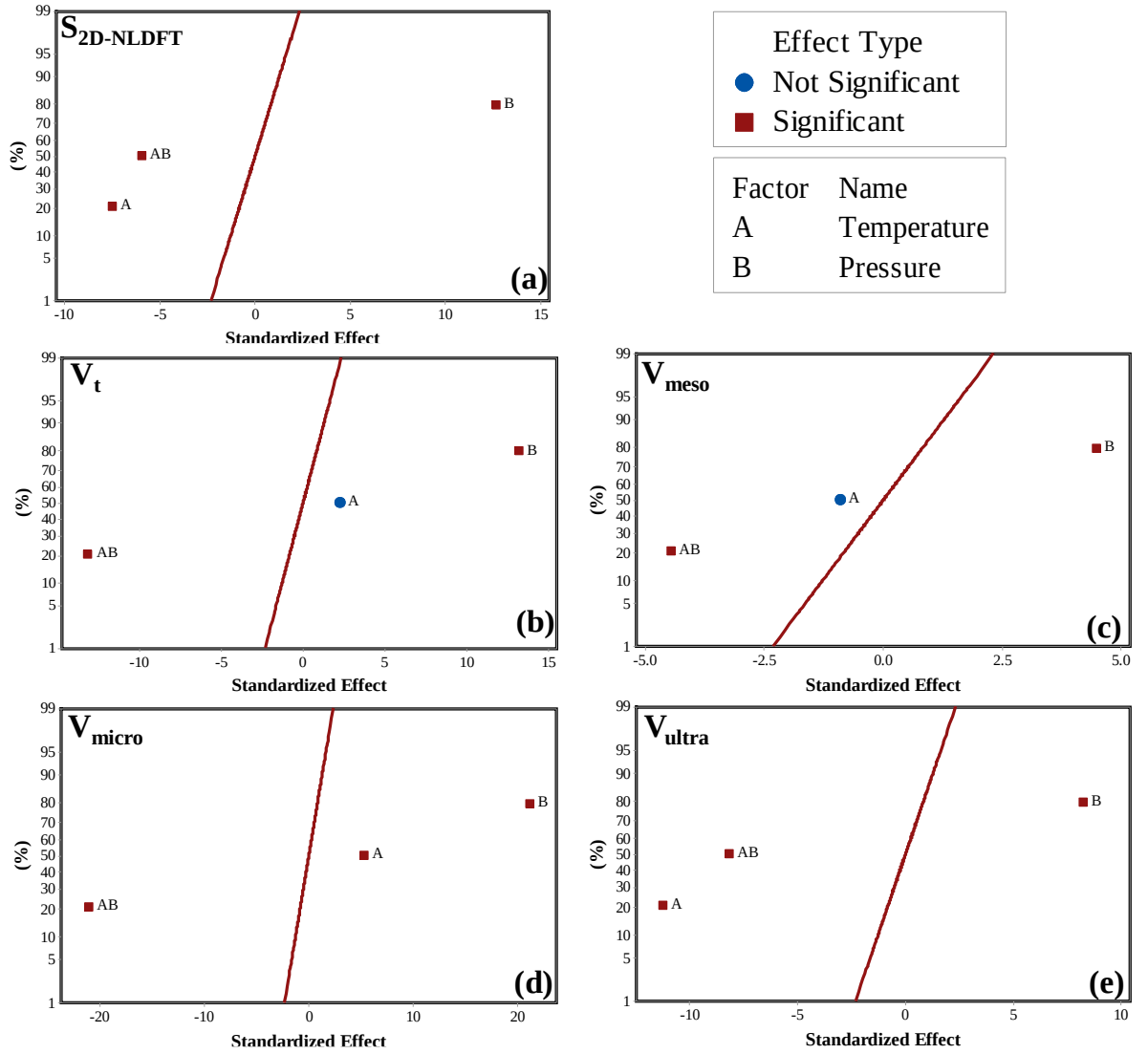

Fig. 2. Normal plots of standardized effects (α = 0.05) for physically activated biochars: specific surface area (a); total pore volume (b); mesopore volume (c); micropore volume (d); ultra-micropore volume (e).

The specific surface areas reported in Table 3 were in line with expectations, given the present activation conditions. Even at the lowest temperatures (700 °C) it was possible to obtain relatively high surface areas, even greater than those measured for activated biochars produced at higher temperatures. As can be seen in Fig. 2a, the specific surface area was positively influenced by the absolute pressure and negatively affected by the activation temperature. Especially at 1.0 MPa, relatively low temperatures and longer activation times allowed the biochar to be gasified more homogeneously, thus resulting in a more developed porous

structure. Conversely, higher temperatures led to faster reaction rates, which can result in a more severe enlargement of micropores and the subsequent loss of surface area.

Fig. 2b shows that the total pore volume increased significantly when the pressure was raised from 0.1 to 1.0 MPa. In general, the total pore volumes for physically activated biochars, which were not significantly affected by the activation temperature, were higher than those measured for chemically activated carbons. As can be seen when comparing the data reported in Tables 2 and 3, physical activation led to porous carbons with slightly higher ultra-micropore volumes. An inspection of Figs. 2d, 2e and A.3b reveals that high temperatures can lead to some widening of the narrowest micropores, since the activation temperature had a negative effect on the ultra-micropore volumes and a positive one on the micropore volumes. With regards to the volume of mesopores, which was mainly affected by pressure (see Fig. 2c), it should be noticed that physical activation under pressure resulted in more hierarchical porous structures with higher contributions of mesopores (see values of V_{meso} and relative percentages in Table 3). The statistically significant overall curvature terms reported in Table A.3 for $S_{2D\text{-}NLDFT}$, V_t, V_{meso}, and V_{micro} response variables also suggest that a central composite design could be required for optimization purposes.

Given the significant effects of pressure on the textural properties of carbons activated at 700−850 °C, we decided to perform two additional physical activations at 650 °C, leading to the materials called PB_650_0.10 and PB_650_1.00. The results obtained, which are also reported in Table 3, seem to confirm that activation with CO_2 under pressure is a very interesting way to produce biomass-derived porous carbons with high specific surface area and wide pore size distributions (including relatively high mesopore volumes), even at relatively low temperatures.

3.3. Catalytic activity

Due to their relatively high specific surface area, both PB_700_1.00 and CB_3_0.10 activated biochars (one for each activation procedure) were selected as catalysts and tested during the upgrading process of the aqueous phase of a real pyrolysis oil.

Elemental and moisture analyses of the aqueous phase of the pyrolysis oil revealed that the liquid sample had an average chemical formula of $C_5 H_{6.7} O_2$ and a water content of 80 wt. %. Since the liquid was fed to the reformer without providing additional water, the steam to carbon molar ratio, S:C, was 4:1.

It is generally assumed that deactivation and/or instability of the catalyst can be attributed to two different phenomena: (1) the deposition of carbonaceous material (coke) on the surface of the catalyst, which clogs part of the available active sites; and (2) the extent of gasification reactions (both with steam and CO_2) of the carbon-based catalyst, which leads to a loss of mass and a subsequent increase in LHSV (i.e., less contact time).

The results obtained in terms of total gas yield, selectivity towards specific gaseous species, hydrogen yield and hydrogen release over time are displayed in Fig. 3a. It should be noted that the poor results measured for the blank test (i.e., empty reactor) suggested that the reactor wall did not play a crucial catalytic role. The physically activated biochar (PB_700_1.00) exhibited performances comparable to those obtained in a previous study [33]. Using this material, which showed a good stability during the whole experiment (see Fig. 3b), a total gas yield of about 40% was obtained. Nevertheless, its relatively low hydrogen yield indicates that the extent of steam reforming was modest.

Regarding the performance of the chemically activated biochar (CB_3_0.10), a similar total gas yield was measured, compared to the physically activated one. However, selectivity to gaseous products were markedly different, leading to a decrease in the production of H_2 (the hydrogen yield was even lower than that of PB_700_1.00) and an increase in that of CO_2. This

result could suggest that the decomposition of pyrolysis oil instead of steam and/or dry reforming, was the main process involved.

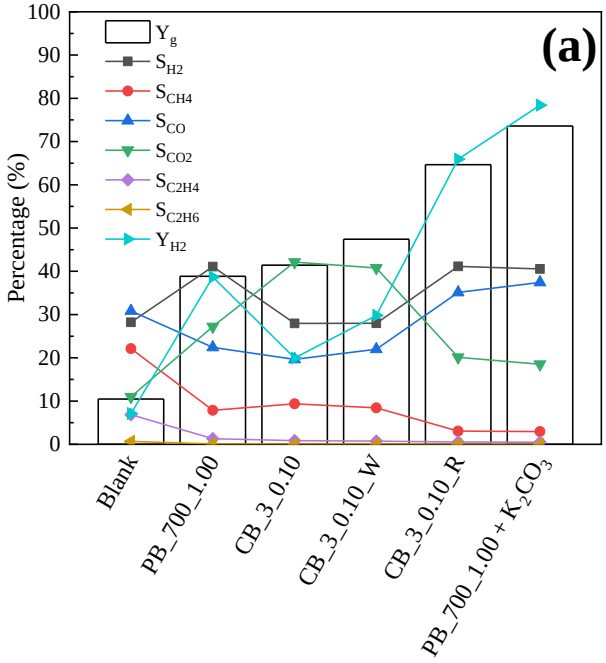

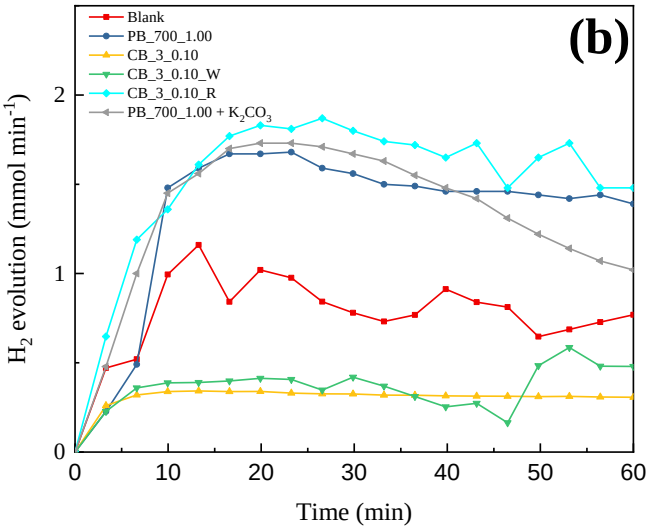

Fig. 3. Results obtained from combined steam and dry reforming of pyrolysis oil at 750°C: total and H_2 yields (Y_g and Y_{H2}, respectively) as well as selectivities toward a given gaseous product, S_i (a); and evolution of the hydrogen production rate (b).

As can be deduced from Fig. 3a, similar results were also obtained for the chemically activated biochar that was washed with just water (CB_3_0.10_W). The differences in the performance

between the physically and chemically activated biochars could be related to their textural properties. In this respect, the physically activated biochar exhibited a higher specific surface area and higher volumes of micro- and mesopores, thus providing more catalytic active sites of inherent alkali or alkaline earth metal species (AAEMs). The catalytic role of these species (especially K, Mg and Ca) in both steam reforming and gasification of carbon has been widely reported [25,44–46]. Furthermore, the more hierarchical pore size distribution of PB_700_1.00, with relatively high contributions of the mesopores, could shorten the diffusion path to reach the active sites.

Fig. 3b clearly shows that H_2 release rates fluctuated over time for most of biochars tested. There are at least two possible explanations for this: First, the coke deposits, which gradually covered the catalyst surface, could have ted to large fluctuations in the extent of the reactions involved. Second, the structural modification of the activated carbons (the process temperature was higher than the activation temperature) could also led to unsteady hydrogen flow rates at the outlet. It should be noted that the reaction system studied was certainly complex, due the numerous competitive reactions that can affect the yields of the different gaseous products. Nevertheless, it can be assumed that methane is mainly produced by the cracking of the heaviest fraction of the pyrolysis oil, and that its yield will be correlated to the amount of coke produced [47]. Similarly, Fig. 3a reveals that the selectivity towards methane was almost constant for PB_700_1.00, CB_3_0.10, and CB_3_0.10_W materials. Therefore, it can be concluded that the coke production in the process was quite similar for the above-mentioned carbons, suggesting that some structural modifications in the carbons could be accounted for the unsteady production of hydrogen. These modifications could be ascribed to the reverse Boudouard reaction [48,49], steam gasification and, in the case of the chemical activated biochars, potassium-catalyzed gasification. To support this argument, Fig. 4 shows the textural properties of fresh and spent activated biochars. Contrary to the loss of porosity observed for

453 spent PB_700_1.00 and CB_3_0.10 catalysts, the spent CB_3_0.1_W material showed an
454 increase in pore volumes, especially for micropores. In addition, the results from TPD
455 measurements, which are summarized graphically in Figs. 5 and A.6, indicate that the water-
456 washed chemically activated carbon exhibited a larger mass loss (with an increased release of
457 CO_2 and CO, as shown in Fig. A.6) than that of the acid-washed carbon, thus confirming a
458 greater extent of carbon gasification. This fact could be attributed to the residual amount of
459 activation reagent available on the surface of the catalyst CB_3_0.10_W, which might promote
460 further biochar gasification during the experiment, as recently reported by Wang *et al.* [11].
461 To understand better the effect of the washing procedure on the performance of chemically
462 activated biochars, an unwashed (raw) material (CB_3_0.10_R) was also tested as catalyst. In
463 this case, the total gas yield was 65% with enhanced selectivity towards both H_2 and CO (see
464 Fig. 3a), thus indicating a higher extent of the steam reforming reactions (leading to a Y_{H2} of
465 66%). Fig. 6 displays the FTIR spectra obtained for fresh and spent chemically activated
466 biochars as well as for pure K_2CO_3. In the case of acid and water-washed samples, no evident
467 K_2CO_3 content was detected on the surface, indicating the effectiveness of both washing
468 procedures. On the other hand, most of the chemical activating agent available on the surface
469 of the fresh CB_3_0.10_R catalyst disappeared after the catalytic test. The potassium carbonate
470 (and other chemical species derived from its partial decomposition) available on the surface of
471 the catalyst at the beginning of the reforming test (reductive environment) could progressively
472 be reduced to metallic potassium (K^0), leading to a further promotion of reforming reactions.
473 Furthermore, a process temperature relatively close to the volatilization point of potassium can
474 enhance the mobility and reactivity of the metal [50]. Generally speaking, activated biochars
475 have relatively abundant oxygen and nitrogen-containing functional groups, which are not
476 present in the materials shown in Fig. 6. The reason behind this could be the relatively high
477 activation temperatures, since the majority of functional groups decompose below 800 °C [51].

Furthermore, the relatively high amount of K_2CO_3 loaded on the analyzed samples resulted in a very large peak, which may hide other peaks of interest, such as those related to oxygenated functionalities.

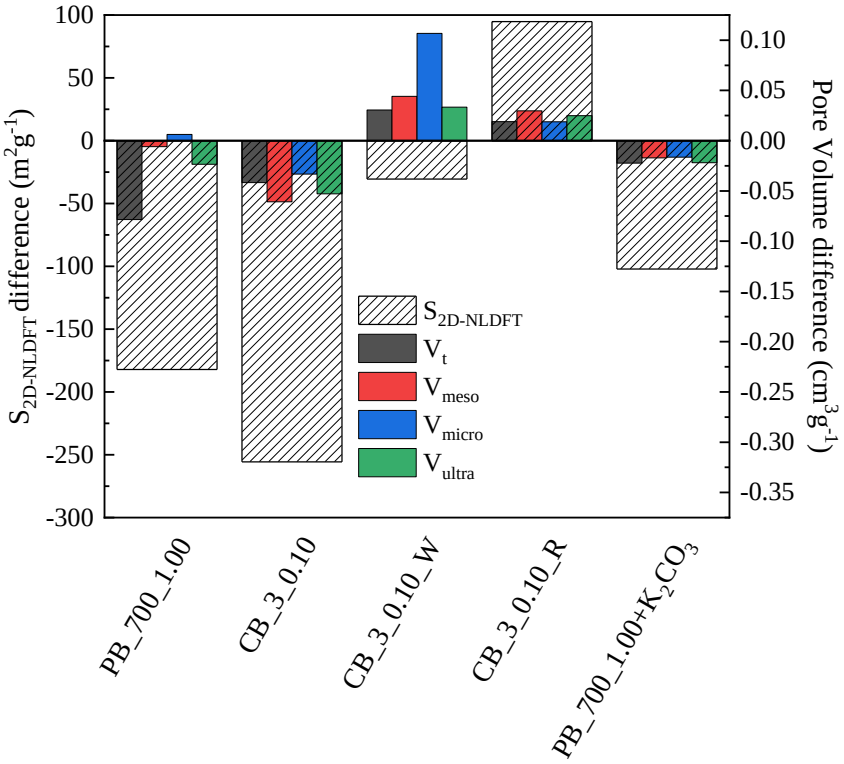

Fig. 4. Differences in textural properties between the fresh and spent activated biochars used as catalysts in steam and dry reforming tests.

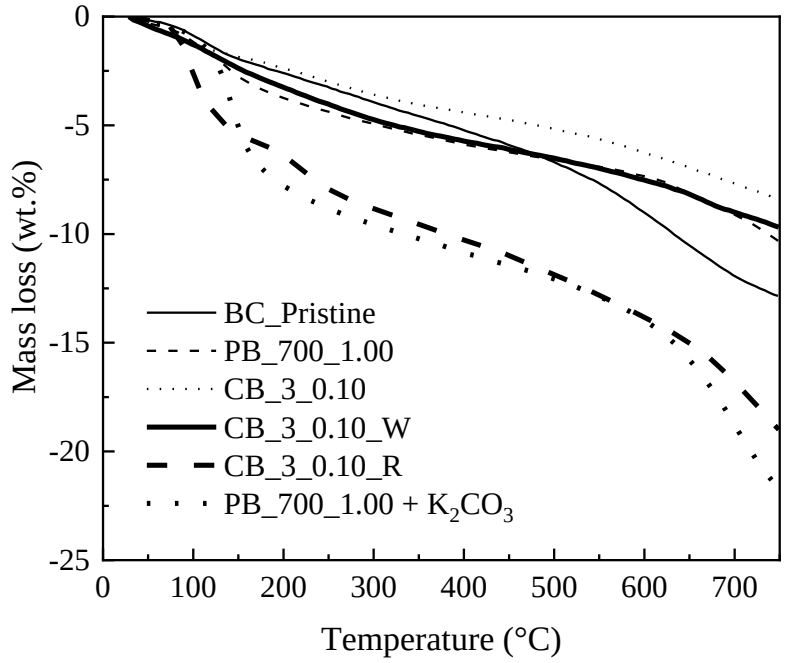

485

486 **Fig. 5**. Results from TPD characterization (percentage of mass loss vs. temperature) for pristine

487 and activated biochars.

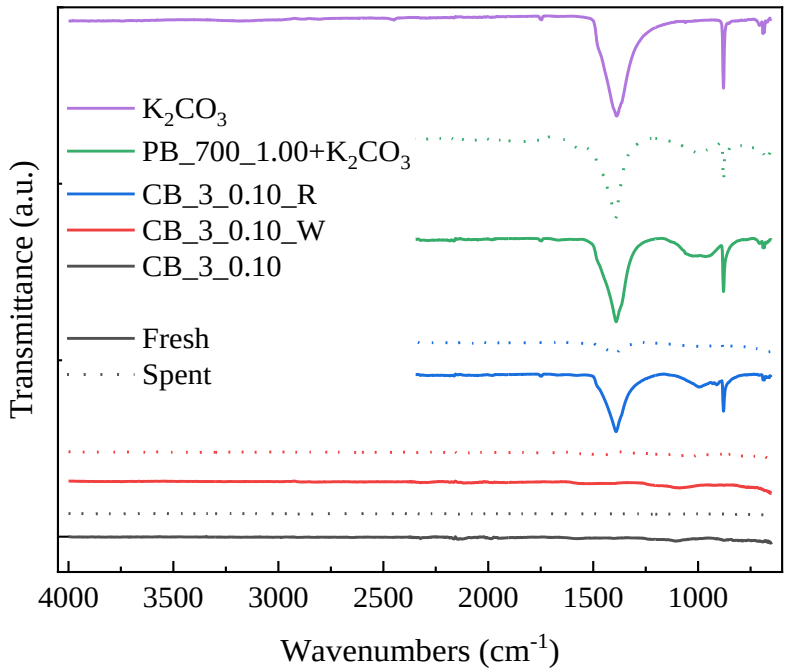

488

489 **Fig. 6**. Comparison of the FTIR spectra obtained for pure K_2CO_3 and some activated biochars

490 tested in the present study.

The results from TPD measurements (see Fig. 5) showed that the mass loss under an inert atmosphere was much higher for the unwashed catalyst. In addition, the release of CO during TPD also increased for the material CB_3_0.10_R (see Fig. A.6c). The increase in both mass loss and CO production when heating in N_2 up to 750 °C could be due to the reaction of K_2CO_3 with carbon, which results in an additional release of CO, especially at temperatures near 700 °C and above, and the formation of catalytically active COK and CK complexes [52]. Hence, a certain gasification of carbon during the catalytic upgrading tests should be expected. In line with this, Fig.4 shows that the spent CB_3_0.10_R exhibited more developed textural properties than the fresh one (for instance, the specific surface area increased from 29 $m^2\ g^{-1}$ to 124 $m^2\ g^{-1}$), thus confirming the extent of gasification reactions. Despite the loss of catalyst through carbon gasification, which results in a higher LHSV, the production rate of H_2 for this catalyst was relatively stable during the experiment. This could be explained by the fact that the carbon gasification catalyzed by K_2CO_3 contributes to creating new pores and then counterbalancing the deposition of coke, which induces micropore blockage and active sites coverage.

Based on the findings discussed above, it seems reasonable to assume that an activated biochar having a wider hierarchical pore size distribution and some availability of K_2CO_3 on its surface appears as an excellent candidate for catalytic pyrolysis vapors upgrading. With this in mind, a new biochar-derived material, designated as PB_700_1.00+K_2CO_3, was prepared by impregnating the material PB_700_1.00 with K_2CO_3 at a mass ratio of carbonate to precursor of 3:1. It should be expected that the better textural properties of the starting physically activated biochar could lead to a more homogeneous dispersion of the active phase on the carbon support, thus resulting in an improved performance of the catalyst.

The results obtained for the catalyst PB_700_1.00+K_2CO_3 confirmed our expectation. The total gas yield reached a maximum value of 74%, whereas the hydrogen yield was the highest

reported in the present study (78%). From the FTIR spectra given in Fig. 6, it can be seen that a fraction of K_2CO_3 was still present on the catalyst surface after running the test.

XPS analyses were carried out for both PB_700_1.00 and PB_700_1.00+K_2CO_3 materials to get additional insight into the role of K_2CO_3 during the pyrolysis vapors upgrading process. From the summarized XPS results given in Table 4, it can be observed that the atomic composition of PB_700_1.00 remained relatively constant after the catalytic test, even though the simultaneous increase of the peaks related to CII and OII seemed to indicate the formation of phenolic groups on the catalysts. The comparison of the atomic compositions between the fresh and spent PB_700_1.00+K_2CO_3 materials indicates that the extent of carbon gasification reactions was much higher than that of the PB_700_1.00 material. Furthermore, from the spectra displayed in Fig. A.7, an additional peak at 283 eV, which is attributed to KC_x carbides, was observed for the spent PB_700_1.00+K_2CO_3. On the other hand, the K2p3/2 region presented only a contribution and suggested the presence of potassium on the surface as K_2O or K_2O_2, according to Li *et al.*[53]. This fact was also confirmed by the shift to lower binding energies of the OII and OIII peaks (see Fig. A.7). The marked difference in the potassium content between fresh and spent PB_700_1.00+K_2CO_3 was probably due to the migration of the potassium-based compounds from the internal pores to the external surface, which can lead to the formation of a coating layer composed of K_2O, as confirmed by SEM-EDX images reported in Fig. 7. The presence of potassium oxides on the surface of the catalyst can be ascribed to (*i*) the direct decomposition of the carbonate (Reaction 7) and/or (*ii*) the formation of metallic potassium. The latter can migrate from the inner structure of the catalyst to its surface during the course of the pyrolysis vapors upgrading tests and finally be oxidized when the catalyst has been removed from the reactor. This fact can also justify the significant decrease in the specific surface area reported in Fig. 4 for the spent PB_700_1.00+K_2CO_3 catalyst (from 130 to 27.7 m^2g^{-1}).

From the SEM-EDX analyses, it can also be deduced that a relatively homogeneous dispersion of K_2CO_3 was achieved for the fresh catalyst. Nevertheless, both fresh and spent catalysts exhibited some clusters and snail shell-like agglomerates, which could be attributed to the relatively high load of carbonate. However, no visible surface carbon layers was found on the superficial K_2O of the spent catalyst, thus suggesting that the extent of the carbon gasification was probably sufficient to prevent the deposition of coke on the surface.

Table 4. Surface composition measured by XPS and peak contributions of C1s, O1s and K2p.

Sample	Surface concentration (at. %)			Binding energies (eV) and relative peak areas (%)[e]								
				C1s region					O1s region			K2p3/2 region
	C	O	K	CI	CII	CIII	CIV	Carbide	OI	OII	OIII	K-O
PB_700_1.00 (Fresh)	87.3	11.3	1.4	284.4 (68.5)	285.7 (23.8)	287.6 (6.3)	289.2 (1.3)		531.1 (30.7)	532.8 (55.4)	534.5 (13.9)	293.3 (100)
PB_700_1.00 (Spent)	82.8	15.1	2.1	284.5 (62.7)	285.5 (31.3)	287.6 (4.1)	289.4 (1.9)		531.3 (20.0)	532.9 (60.2)	534.5 (19.8)	293.7 (100)
PB_700_1.00+K_2CO_3 (Fresh)	72.6	21.6	5.8	284.6 (47.3)	285.8 (40.6)	287.6 (11.0)	289.3 (1.1)		531.3 (12.0)	532.7 (50.5)	534.5 (37.5)	293.7 (100)
PB_700_1.00+K_2CO_3 (Spent)	42.0	27.8	30.2	284.5 (64.2)			288.7 (22.5)	283.1 (22.5)	531.1 (57.9)			292.8 (100)

[e] C1s binding energies in carbon materials: **CI**, hydrocarbons, aromatics, aliphatics (284.5 eV); **CII**, single bond C-O associated to alcohols, phenols, carboxyls (286 eV); **CIII**, double bond C=O in carbonyl, quinone (287.5 eV); **CIV**, carboxyl and carbonate groups (288.7 eV).
O1s binding energies in carbon materials: **OI**, C= O quinone type groups (around 531 eV); **OII**, C–OH phenol groups and/or C–O–C ether groups (532.5 eV), **OIII**, chemisorbed oxygen (COOH carboxylic groups) and/or water (535 eV).

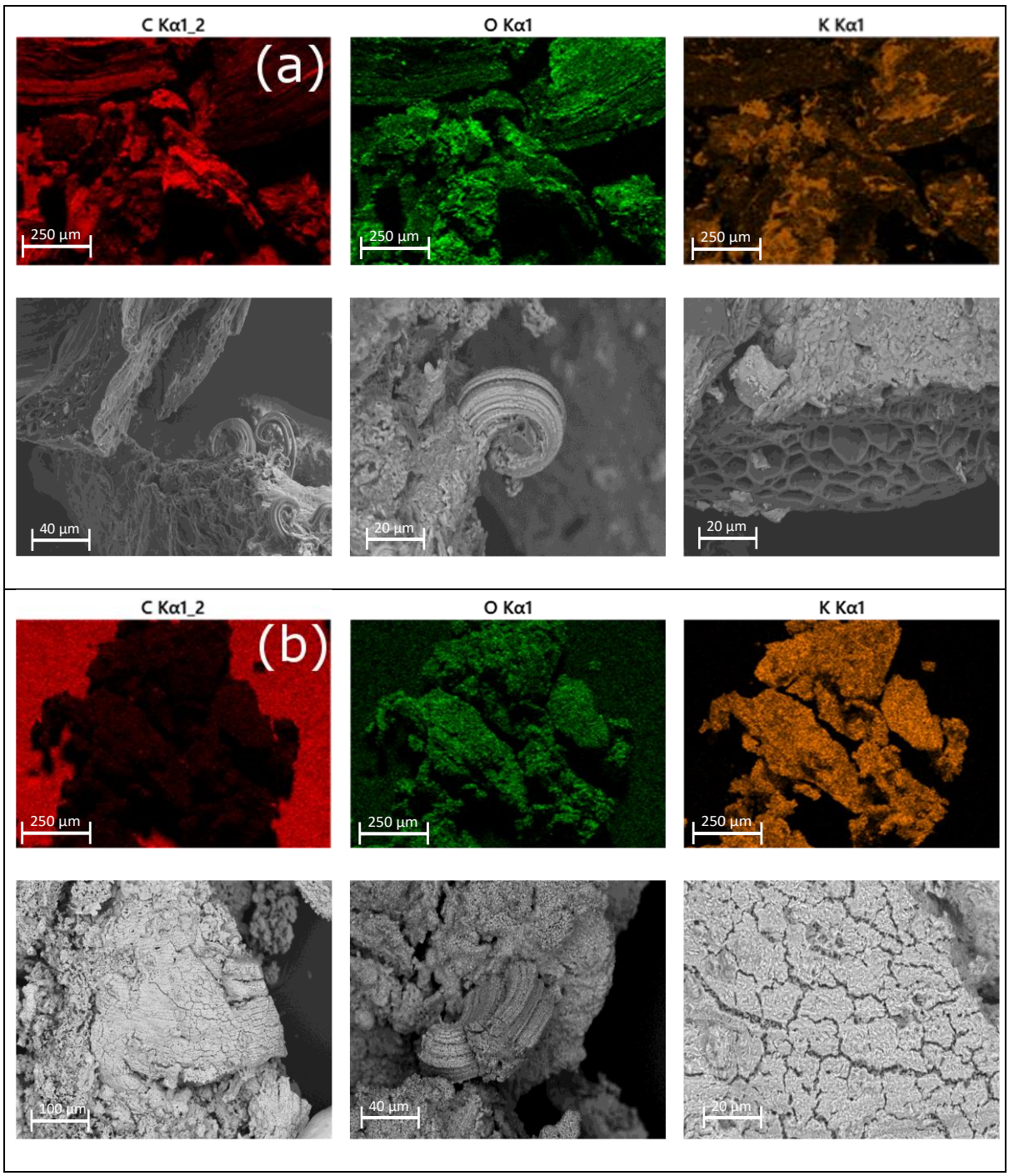

554 **Fig. 7**. SEM-EDX images of fresh (a) and spent (b) PB_700_1.00+K_2CO_3 catalyst.

555 **4. Conclusions**

556 From the results obtained in this study, the following conclusions can be drawn:

557 1. The chemical activation of the pristine biochar led to carbonaceous solids with a
558 relatively high specific surface area and well-developed microporous structure. The

most important activation parameter was found to be the amount of activation agent, which accounted for the development of the porous structure. Activation pressure, on the other hand, was not significant for the outcomes of the procedure. Regarding the washing efficiency, acid washing resulted to be effective in cleaning the surface of the samples, whereas washing with water was not sufficient to remove completely the residual reactants, partially clogging the porosity of the samples.

2. Physical activation was found to be more sensitive to the process parameters. It was possible to obtain acceptable values of specific surface area even at low temperature (650 °C) by increasing the activation pressure to 1.00 MPa. A negative effect of the activation temperature on the results was also observed. In fact, the surface area decreased with the increase in the activation temperature, probably due to the widening of the smaller pores by a too rapid (and thus less controlled) gasification.
3. The most promising material produced by physical or chemical activation (PB_700_1.00 and CB_3_0.10) were tested as catalysts in the upgrading of the aqueous fraction of a real pyrolysis oil. Both activated biochars, which were initially characterized by a well-developed porosity, did not exhibit good performance, showing a huge decrease in the specific surface area, probably due to coke deposition. Nevertheless, the addition of K_2CO_3 to the best physically activated biochar boosted the overall performance towards the production of more hydrogen, as a consequence of the enhanced reforming of pyrolysis oil. This finding can be related to the availability of K^0, which was formed from the decomposition of the K_2CO_3 previously deposited on the activated biochar.

Acknowledgments

This project received funding from the European Union's Horizon 2020 research and innovation programme under the Marie Skłodowska-Curie grant agreement No 721991. The authors also acknowledge the funding from the Aragón Government (Ref. T22_20R), co-funded by FEDER 2014-2020 "Construyendo Europa desde Aragón". ". This study was partly supported by the French PIA project "Lorraine Université d'Excellence", reference ANR-15-IDEX-04-LUE, PROMOTEE project and TALiSMAN project, funded by FEDER (2019-000214). The authors gratefully thank José Antonio Manso (UNIZAR) and Philippe Gadonneix (IJL) for their help in the preparation and characterization of the samples and Sandrine Mathieu (IJL) for the SEM characterization.

Appendix A. Supplementary data

Further details on characterization of pristine and activated biochars. Statistical outcomes from the adopted designs of experiments.

Nomenclature

A_{BET}	Brunauer-Emmett-Teller area ($m^2\ g^{-1}$)
d_p	Pore diameter (nm)
F_{BO}	Molar flow rate of dry bio oil (mol min^{-1})
$F_{H2\ Av}$	Experimental average H_2 molar flow rate (mol min^{-1})
$F_{H2\ Stoi}$	H_2 stoichiometric molar flow rate (mol min^{-1})
m_0	Initial mass of biochar before activation (g)
m_c	Biochar mass before the washing step (g)
m_f	Final mass of biochar after activation (g)

604	m_g	Total mass of produced gas during the upgrading process (g)
605	m_l	Mass of liquid fed into the upgrading reactor (g)
606	m_w	Biochar mass after the washing step (g)
607	n_i	Produced amount of a given gaseous specie i (mol)
608	n_{tot}	Total amount of produced gas (mol)
609	$S_{2D\text{-}NLDFT}$	2D-NLDFT specific surface area ($m^2\ g^{-1}$)
610	S_i	Selectivity toward a given gaseous specie *i* (%)
611	$V_{0.97}$	Gurvitch pore volume ($cm^3\ g^{-1}$)
612	V_{meso}	Volume of mesopores ($cm^3\ g^{-1}$)
613	V_{micro}	Volume of micropores ($cm^3\ g^{-1}$)
614	V_t	Total pore volume ($cm^3\ g^{-1}$)
615	V_{ultra}	Volume of ultra-micropores ($cm^3\ g^{-1}$)
616	Y_g	Total gas yield (%)
617	Y_{H2}	Hydrogen yield (%)
618	Y_{wash}	Washing yield (%)
619	η	Degree of burnout (%)
620	*Acronyms*	
621	FTIR	Fourier-Transform Infrared spectroscopy
622	GHSV	Gas hourly space velocity
623	LHSV	Liquid hourly space velocity

PSD	Pore size distribution
RSM	Response surface methodology
S:C	Steam to carbon molar ratio
STP	Standard temperature and pressure
TPD	Temperature-programmed desorption
XPS	X-ray photoelectron spectroscopy
μ-GC	Micro gas chromatograph

References

[1] Guedidi H, Lakehal I, Reinert L, Lévêque JM, Bellakhal N, Duclaux L. Removal of ionic liquids and ibuprofen by adsorption on a microporous activated carbon: Kinetics, isotherms, and pore sites. Arab J Chem 2020;13:258–70. https://doi.org/10.1016/j.arabjc.2017.04.006.

[2] Santoyo-Cisneros R, Rangel-Mendez JR, Nava JL, Larios-Durán ER, Chazaro-Ruiz LF. Influence of surface chemistry of activated carbon electrodes on electro-assisted adsorption of arsenate. J Hazard Mater 2020;392:122349. https://doi.org/10.1016/j.jhazmat.2020.122349.

[3] Acharya SP, Johnson J, Weidhaas J. Adsorption kinetics of the herbicide safeners, benoxacor and furilazole, to activated carbon and agricultural soils. J Environ Sci (China) 2020;89:23–34. https://doi.org/10.1016/j.jes.2019.09.022.

[4] Palomo J, Rodríguez-Cano MA, Rodríguez-Mirasol J, Cordero T. On the kinetics of methanol dehydration to dimethyl ether on Zr-loaded P-containing mesoporous activated carbon catalyst. Chem Eng J 2019;378:122198. https://doi.org/10.1016/j.cej.2019.122198.

[5] Liu WJ, Jiang H, Yu HQ. Development of Biochar-Based Functional Materials: Toward a Sustainable Platform Carbon Material. Chem Rev 2015;115:12251–85. https://doi.org/10.1021/acs.chemrev.5b00195.

[6] Wang Y, Yang H, Jin L, Li Y, Hu H, Ding H, et al. Effect of mineral in coal on preparation of activated carbon for methane decomposition to hydrogen. Fuel 2019;258:116138. https://doi.org/10.1016/j.fuel.2019.116138.

[7] Li H, Zheng F, Wang J, Zhou J, Huang X, Chen L, et al. Facile preparation of zeolite-activated carbon composite from coal gangue with enhanced adsorption performance. Chem Eng J 2020;390:124513. https://doi.org/10.1016/j.cej.2020.124513.

[8] Ding S, Liu Y. Adsorption of CO2 from flue gas by novel seaweed-based KOH-activated porous biochars. Fuel 2020;260:116382. https://doi.org/10.1016/j.fuel.2019.116382.

[9] Iriarte-Velasco U, Sierra I, Zudaire L, Ayastuy JL. Preparation of a porous biochar from the acid activation of pork bones. Food Bioprod Process 2016;98:341–53. https://doi.org/10.1016/j.fbp.2016.03.003.

[10] Sayğılı H, Akkaya Sayğılı G. Optimized preparation for bimodal porous carbon from lentil processing waste by microwave-assisted K2 CO3 activation : Spectroscopic characterization and dye decolorization activity. J Clean Prod 2019;226:968–76. https://doi.org/10.1016/j.jclepro.2019.04.121.

[11] Wang L, Sun F, Hao F, Qu Z, Gao J, Liu M, et al. A green trace K2CO3 induced catalytic activation strategy for developing coal-converted activated carbon as advanced candidate for CO2 adsorption and supercapacitors. Chem Eng J 2020;383:123205. https://doi.org/10.1016/j.cej.2019.123205.

[12] Mai TT, Vu DL, Huynh DC, Wu NL, Le AT. Cost-effective porous carbon materials synthesized by carbonizing rice husk and K2CO3 activation and their application for lithium-sulfur batteries. J Sci Adv Mater Devices 2019;4:223–9. https://doi.org/10.1016/j.jsamd.2019.04.009.

[13] Lahijani P, Zainal ZA, Mohammadi M, Mohamed AR. Conversion of the greenhouse gas CO2 to the fuel gas CO via the Boudouard reaction: A review. Renew Sustain Energy Rev 2015;41:615–32. https://doi.org/10.1016/j.rser.2014.08.034.

[14] Şahin Ö, Saka C. Preparation and characterization of activated carbon from acorn shell by physical activation with H2O – CO2 in two-step pretreatment. Bioresour Technol 2013;136:163–8. https://doi.org/10.1016/j.biortech.2013.02.074.

[15] Guo Y, Tan C, Sun J, Li W, Zhang J, Zhao C. Porous activated carbons derived from

682 waste sugarcane bagasse for CO2 adsorption. Chem Eng J 2020;381:122736.
683 https://doi.org/10.1016/j.cej.2019.122736.
684 [16] Bertero M, Puente G De, Sedran U. Fuels from bio-oils : Bio-oil production from
685 different residual sources , characterization and thermal conditioning. Fuel
686 2012;95:263–71. https://doi.org/10.1016/j.fuel.2011.08.041.
687 [17] Fu M, Qi W, Xu Q, Zhang S, Yan Y. Hydrogen production from bio-oil model
688 compounds dry (CO2) reforming over Ni/Al2O3 catalyst. Int J Hydrogen Energy
689 2015;41:1494–501. https://doi.org/10.1016/j.ijhydene.2015.11.104.
690 [18] Santamaria L, Artetxe M, Lopez G, Cortazar M, Amutio M, Bilbao J, et al. Effect of
691 CeO2 and MgO promoters on the performance of a Ni/Al2O3 catalyst in the steam
692 reforming of biomass pyrolysis volatiles. Fuel Process Technol 2020;198:106223.
693 https://doi.org/10.1016/j.fuproc.2019.106223.
694 [19] Santamaria L, Lopez G, Arregi A, Amutio M, Artetxe M, Bilbao J, et al. Stability of
695 different Ni supported catalysts in the in-line steam reforming of biomass fast
696 pyrolysis volatiles. Appl Catal B Environ 2019;242:109–20.
697 https://doi.org/10.1016/j.apcatb.2018.09.081.
698 [20] Bimbela F, Ábrego J, Puerta R, García L, Arauzo J. Catalytic steam reforming of the
699 aqueous fraction of bio-oil using Ni-Ce / Mg-Al catalysts. Appl Catal B Environ
700 2017;209:346–57. https://doi.org/10.1016/j.apcatb.2017.03.009.
701 [21] Phongprueksathat N, Meeyoo V, Rirksomboon T. Steam reforming of acetic acid for
702 hydrogenproduction : Catalytic performances of Ni and Co supported on
703 Ce0·75Zr0·25O2 catalysts. Int J Hydrogen Energy 2019;44:9359–67.
704 https://doi.org/10.1016/j.ijhydene.2019.02.085.
705 [22] Domine ME, Iojoiu EE, Davidian T, Guilhaume N, Mirodatos C. Hydrogen production
706 from biomass-derived oil over monolithic Pt- and Rh-based catalysts using steam

reforming and sequential cracking processes. Catal Today 2008;133–135:565–73. https://doi.org/10.1016/j.cattod.2007.12.062.

[23] Li X, Zhang Z, Zhang L, Fan H, Li X, Liu Q, et al. Investigation of coking behaviors of model compounds in bio-oil during steam reforming. Fuel 2020;265:116961. https://doi.org/10.1016/j.fuel.2019.116961.

[24] Ma Z, Xiao R, Zhang H. Catalytic steam reforming of bio-oil model compounds for hydrogen-rich gas production using bio-char as catalyst. Int J Hydrogen Energy 2016;42:3579–85. https://doi.org/10.1016/j.ijhydene.2016.11.107.

[25] Feng D, Zhao Y, Zhang Y, Sun S, Meng S, Guo Y, et al. Effects of K and Ca on reforming of model tar compounds with pyrolysis biochars under H2O or CO2. Chem Eng J 2016;306:422–32. https://doi.org/10.1016/j.cej.2016.07.065.

[26] Buentello-Montoya D, Zhang X, Li J, Ranade V, Marques S, Geron M. Performance of biochar as a catalyst for tar steam reforming: Effect of the porous structure. Appl Energy 2020;259:114176. https://doi.org/10.1016/j.apenergy.2019.114176.

[27] Feng D, Zhao Y, Zhang Y, Zhang Z, Sun S. Roles and fates of K and Ca species on biochar structure during in-situ tar H2O reforming over nascent biochar. Int J Hydrogen Energy 2017;42:21686–96. https://doi.org/10.1016/j.ijhydene.2017.07.096.

[28] Zhang Z, Ou Z, Qin C, Ran J, Wu C. Roles of alkali/alkaline earth metals in steam reforming of biomass tar for hydrogen production over perovskite supported Ni catalysts. Fuel 2019;257:116032. https://doi.org/10.1016/j.fuel.2019.116032.

[29] Megaritis A, Zhuo Y, Messenböck R, Dugwell DR, Kandiyoti R. Pyrolysis and gasification in a bench-scale high-pressure fluidized-bed reactor. Energy Fuels 1998;12:144–51. https://doi.org/10.1021/ef970115x.

[30] Dufour A, Celzard A, Fierro V, Martin E, Broust F, Zoulalian A. Catalytic decomposition of methane over a wood char concurrently activated by a pyrolysis gas.

Appl Catal A Gen 2008;346:164–73. https://doi.org/10.1016/j.apcata.2008.05.023.

[31] Ranguin R, Jean-Marius C, Yacou C, Gaspard S, Feidt C, Rychen G, et al. Reduction of chlordecone environmental availability by soil amendment of biochars and activated carbons from lignocellulosic biomass. Environ Sci Pollut Res 2020. https://doi.org/10.1007/s11356-019-07366-2.

[32] Greco G, Videgain M, Di Stasi C, González B, Manyà JJ. Evolution of the mass-loss rate during atmospheric and pressurized slow pyrolysis of wheat straw in a bench-scale reactor. J Anal Appl Pyrolysis 2018;136:18–26. https://doi.org/10.1016/j.jaap.2018.11.007.

[33] Di Stasi C, Alvira D, Greco G, González B, Manyà JJ. Physically activated wheat straw-derived biochar for biomass pyrolysis vapors upgrading with high resistance against coke deactivation. Fuel 2019;255:115807. https://doi.org/10.1016/j.fuel.2019.115807.

[34] Jagiello J, Kenvin J, Celzard A, Fierro V. Enhanced resolution of ultra micropore size determination of biochars and activated carbons by dual gas analysis using N2 and CO2 with 2D-NLDFT adsorption models. Carbon 2019;144:206–15. https://doi.org/10.1016/j.carbon.2018.12.028.

[35] Sanchez-Sanchez A, Izquierdo MT, Medjahdi G, Ghanbaja J, Celzard A, Fierro V. Ordered mesoporous carbons obtained by soft-templating of tannin in mild conditions. Microporous Mesoporous Mater 2018;270:127–39. https://doi.org/10.1016/j.micromeso.2018.05.017.

[36] Matos J, Labady M, Albornoz A, Laine J, Brito JL. Catalytic effect of KOH on textural changes of carbon macro-networks by physical activation. J Mol Catal A Chem 2005;228:189–94. https://doi.org/10.1016/j.molcata.2004.09.039.

[37] Lozano-Castelló D, Calo JM, Cazorla-Amorós D, Linares-Solano A. Carbon activation

with KOH as explored by temperature programmed techniques, and the effects of hydrogen. Carbon 2007;45:2529–36. https://doi.org/10.1016/j.carbon.2007.08.021.

[38] Ganga Devi T, Kannan MP. Calcium catalysis in air gasification of cellulosic chars. Fuel 1998;77:1825–30. https://doi.org/10.1016/S0016-2361(98)00038-6.

[39] Dehkhoda AM, Gyenge E, Ellis N. A novel method to tailor the porous structure of KOH-activated biochar and its application in capacitive deionization and energy storage. Biomass Bioenergy 2016;87:107–21. https://doi.org/10.1016/j.biombioe.2016.02.023.

[40] Malekshahian M, Hill JM. Effect of pyrolysis and CO2 gasification pressure on the surface area and pore size distribution of petroleum coke. Energy Fuels 2011;25:5250–6. https://doi.org/10.1021/ef201231w.

[41] Montané D, Fierro V, Marêché JF, Aranda L, Celzard A. Activation of biomass-derived charcoal with supercritical water. Microporous Mesoporous Mater 2009;119:53–9. https://doi.org/10.1016/j.micromeso.2008.09.040.

[42] Malekshahian M, Hill JM. Kinetic Analysis of CO2 Gasification of Petroleum Coke at High Pressures. Energy Fuels 2011;25:4043–8. https://doi.org/10.1021/ef2009259.

[43] Fermoso J, Stevanov C, Moghtaderi B, Arias B, Pevida C, Plaza MG, et al. High-pressure gasification reactivity of biomass chars produced at different temperatures. J Anal Appl Pyrolysis 2009;85:287–93. https://doi.org/10.1016/j.jaap.2008.09.017.

[44] Yip K, Tian F, Hayashi JI, Wu H. Effect of alkali and alkaline earth metallic species on biochar reactivity and syngas compositions during steam gasification. Energy Fuels 2010;24:173–81. https://doi.org/10.1021/ef900534n.

[45] Sueyasu T, Oike T, Mori A, Kudo S, Norinaga K, Hayashi JI. Simultaneous steam reforming of tar and steam gasification of char from the pyrolysis of potassium-loaded woody biomass. Energy Fuels 2012;26:199–208. https://doi.org/10.1021/ef201166a.

[46] Jiang L, Hu S, Wang Y, Su S, Sun L, Xu B, et al. Catalytic effects of inherent alkali and alkaline earth metallic species on steam gasification of biomass. Int J Hydrogen Energy 2015;40:15460–9. https://doi.org/10.1016/j.ijhydene.2015.08.111.

[47] Matos J, Laine J. Ethylene conversion on activated carbon-supported NiMo catalysts: Effect of the support. Appl Catal A Gen 2003;241:25–38. https://doi.org/10.1016/S0926-860X(02)00427-1.

[48] Díaz K, García V, Matos J. Activated carbon supported Ni – Ca: Influence of reaction parameters on activity and stability of catalyst on methane reformation. Fuel 2007;86:1337–44. https://doi.org/10.1016/j.fuel.2006.05.011.

[49] Matos J, Díaz K, García V, Cordero TC, Brito JL. Methane transformation in presence of carbon dioxide on activated carbon supported nickel – calcium catalysts. Catalysis Lett. 2006;109:163–169. https://doi.org/10.1007/s10562-006-0073-3.

[50] Ducousso M, Weiss-Hortala E, Lyczko N, Nzihou A, Castaldi MJ. 110th Anniversary: Syngas Production Enhancement Using Calcium- And Potassium-Impregnated Chars. Ind Eng Chem Res 2019;58:15134–41. https://doi.org/10.1021/acs.iecr.9b02238.

[51] Figueiredo JL, Pereira MFR. The role of surface chemistry in catalysis with carbons. Catal Today 2010;150:2–7. https://doi.org/10.1016/j.cattod.2009.04.010.

[52] Kopyscinski J, Rahman M, Gupta R, Mims CA, Hill JM. K2CO3 catalyzed CO2 gasification of ash-free coal. Interactions of the catalyst with carbon in N2 and CO2 atmosphere. Fuel 2014;117:1181–9. https://doi.org/10.1016/j.fuel.2013.07.030.

[53] Li X, Liu J, Kong F, Liu X, Xu J, Chen H. Potassium-doped graphene for simultaneous determination of nitrite and sul fi te in polluted water. Electrochem Commun 2012;20:109–12. https://doi.org/10.1016/j.elecom.2012.04.014.

Appendix A: supplementary material

Influence of activation conditions on textural properties and performance of activated biochars for pyrolysis vapors upgrading

Christian Di Stasi[1*], *Gianluca Greco*[1], *Rafael L. S. Canevesi*[2], *M. Teresa Izquierdo*[3], *Vanessa Fierro*[2], *Alain Celzard*[2], *Belén González*[1], *Joan J. Manyà*[1]

[1] Aragón Institute of Engineering Research (I3A), Technological College of Huesca, University of Zaragoza, crta. Cuarte s/n, Huesca, E-22071, Spain

[2] Université de Lorraine, CNRS, IJL, Épinal, F-88000, France

[3] Instituto de Carboquímica (ICB-CSIC), Miguel Luesma Castán 4, Zaragoza, E-50018, Spain

[*] Corresponding author at: *Aragón Institute of Engineering Research (I3A), Technological College of Huesca, University of Zaragoza, crta. Cuarte s/n, Huesca, E-22071, Spain.*

E-mail address: christiandistasi@unizar.es.

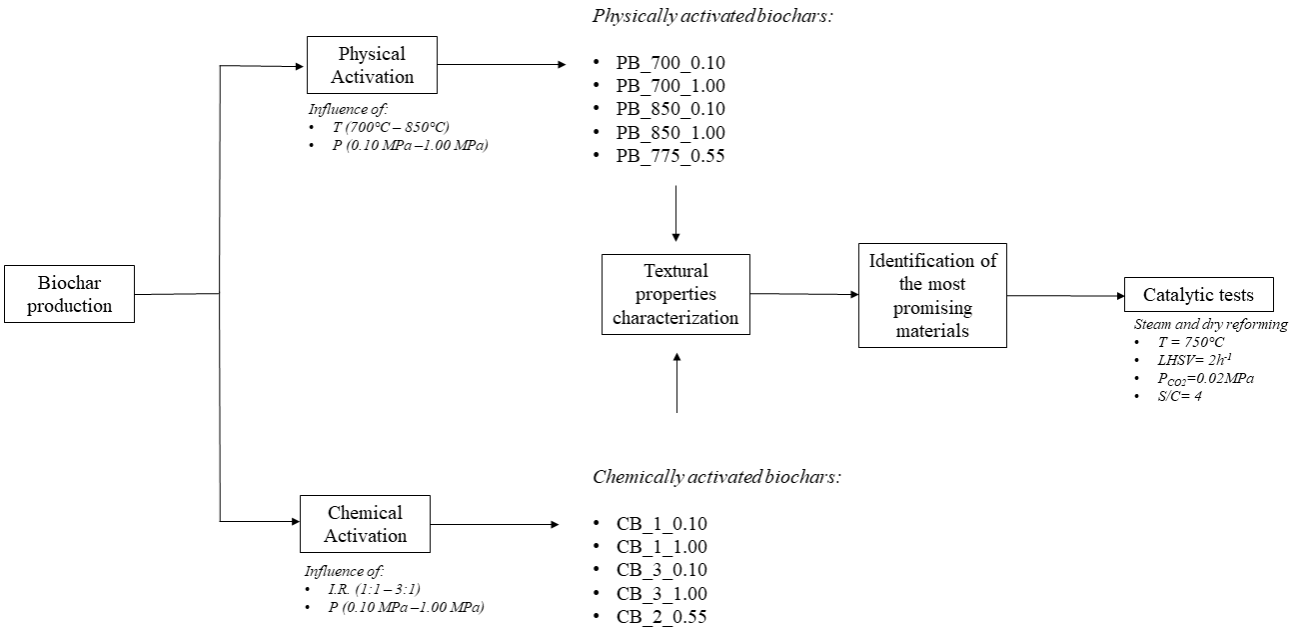

Fig. A.1. Schematic representation of the methodology followed in this study.

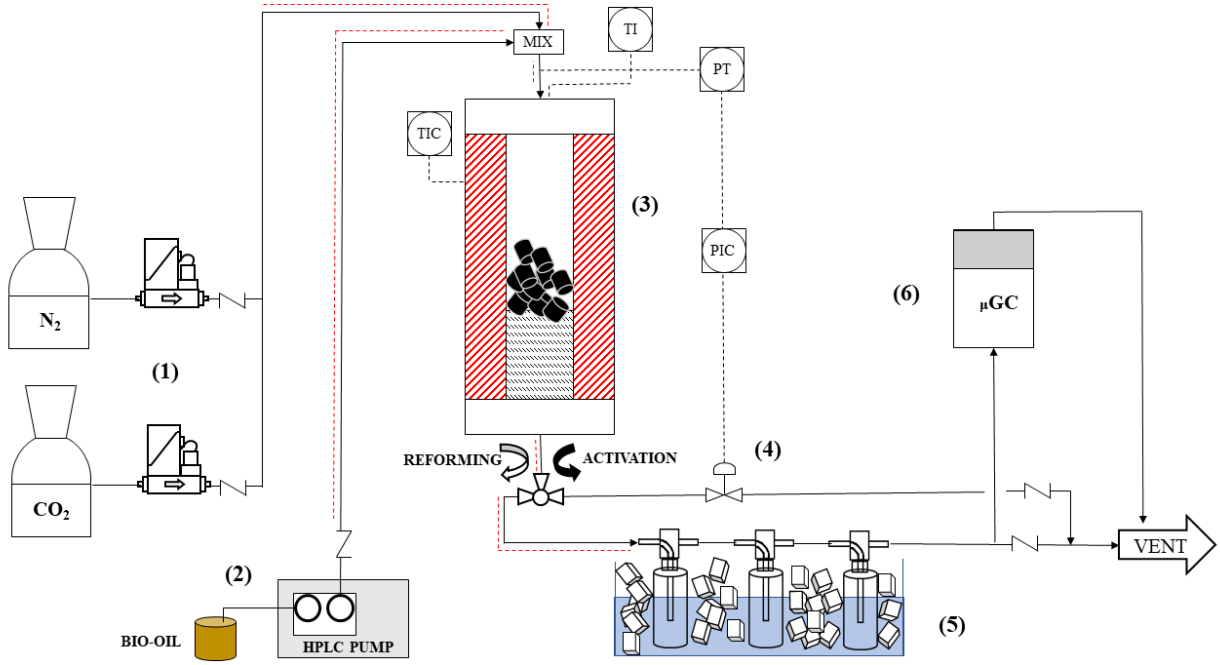

Fig. A.2. Overview of the experimental device used for activation and reforming tests: Feeding system (1); HPLC pump (2); fixed-bed reactor and furnace (3); Servo-controlled valve (4); condensation train (5); and µ-GC analyzer (6).

Table A.1. Results of textural characterization, proximate analysis and elemental analysis of pristine biochar derived from wheat straw

Proximate analysis (wt. %)	
Moisture	2.00 ± 0.08
Volatile matter	10.8 ± 0.63
Ashes	12.7 ± 0.21
Fixed carbon	74.5 ± 0.55
Ultimate (wt. % on a dry ash-free basis)	
C	92.6 ± 0.07
H	4.02 ± 0.05
N	2.01 ± 0.08
O	1.32
Molar H:C ratio	0.52
Textural characterization	
A_{BET} ($m^2\ g^{-1}$)	2.90
$S_{2D\text{-}NLDFT}$ ($m^2\ g^{-1}$)	341
$V_{0.97}$ ($cm^3\ g^{-1}$)	0.0026
V_{tot} ($cm^3\ g^{-1}$)	0.084
V_{ultra} ($cm^3\ g^{-1}$)	0.083
V_{micro} ($cm^3\ g^{-1}$)	0.083
V_{meso} ($cm^3\ g^{-1}$)	0.001 **(1.28 vol. %)**

Table A.2. Regression coefficients and quality-of-fit statistics for the design of experiments on chemical activation. The values in brackets correspond to the *p*-values resulting from the *t*-tests. The significant terms are marked in bold

	Response variable				
	$S_{2D\text{-}NLDFT}$	V_t	V_{meso}	V_{micro}	V_{ultra}
β_0	810.1	0.21605	0.009516	0.2065	0.16447
	(0.000)	(0.000)	(0.003)	(0.000)	(0.000)
β_A (Pressure)	–12.24	–0.00364	0.000215	–0.00385	–0.00553
	(0.326)	(0.132)	(0.715)	(0.190)	(0.150)
β_B (Mass ratio)	**73.32**	**0.02801**	**0.002904**	**0.02511**	**0.01871**
	(0.016)	**(0.003)**	**(0.030)**	**(0.006)**	**(0.016)**
β_{AB}	–36.90	**–0.1089**	–0.000625	–0.01026	–0.00865
	(0.060)	**(0.018)**	(0.346)	(0.035)	(0.070)
R^2_{adj} **(%)**	94.05	98.78	83.90	97.38	93.27
Curvature	**(0.042)**	**(0.015)**	(0.350)	**(0.029)**	(0.090)

Table A.3. Regression coefficients and quality-of-fit statistics for the design of experiments on physical activation. The values in brackets correspond to the *p*-values resulting from the *t*-tests. The significant terms are marked in bold

	Response variable				
	$S_{2D\text{-}NLDFT}$	V_t	V_{meso}	V_{micro}	V_{ultra}
β_0	884.9	0.29181	0.023189	0.268623	0.19055
	(0.000)	(0.000)	(0.001)	(0.000)	(0.000)
β_A (Temperature)	**–35.46**	0.00381	–0.000811	**0.004623**	**–0.01445**
	(0.017)	(0.155)	(0.461)	**(0.034)**	**(0.008)**
β_B (Pressure)	**59.54**	**0.02250**	**0.004000**	**0.018500**	**0.01050**
	(0.006)	**(0.006)**	**(0.047)**	**(0.002)**	**(0.015)**
β_{AB}	**–28.08**	**–0.02250**	**–0.004000**	**–0.018500**	**–0.01050**
	(0.027)	**(0.006)**	**(0.047)**	**(0.002)**	**(0.015)**
R^2_{adj} **(%)**	98.06	98.47	86.47	99.42	98.22
Curvature	**(0.018)**	**(0.025)**	(0.328)	**(0.008)**	**(0.013)**

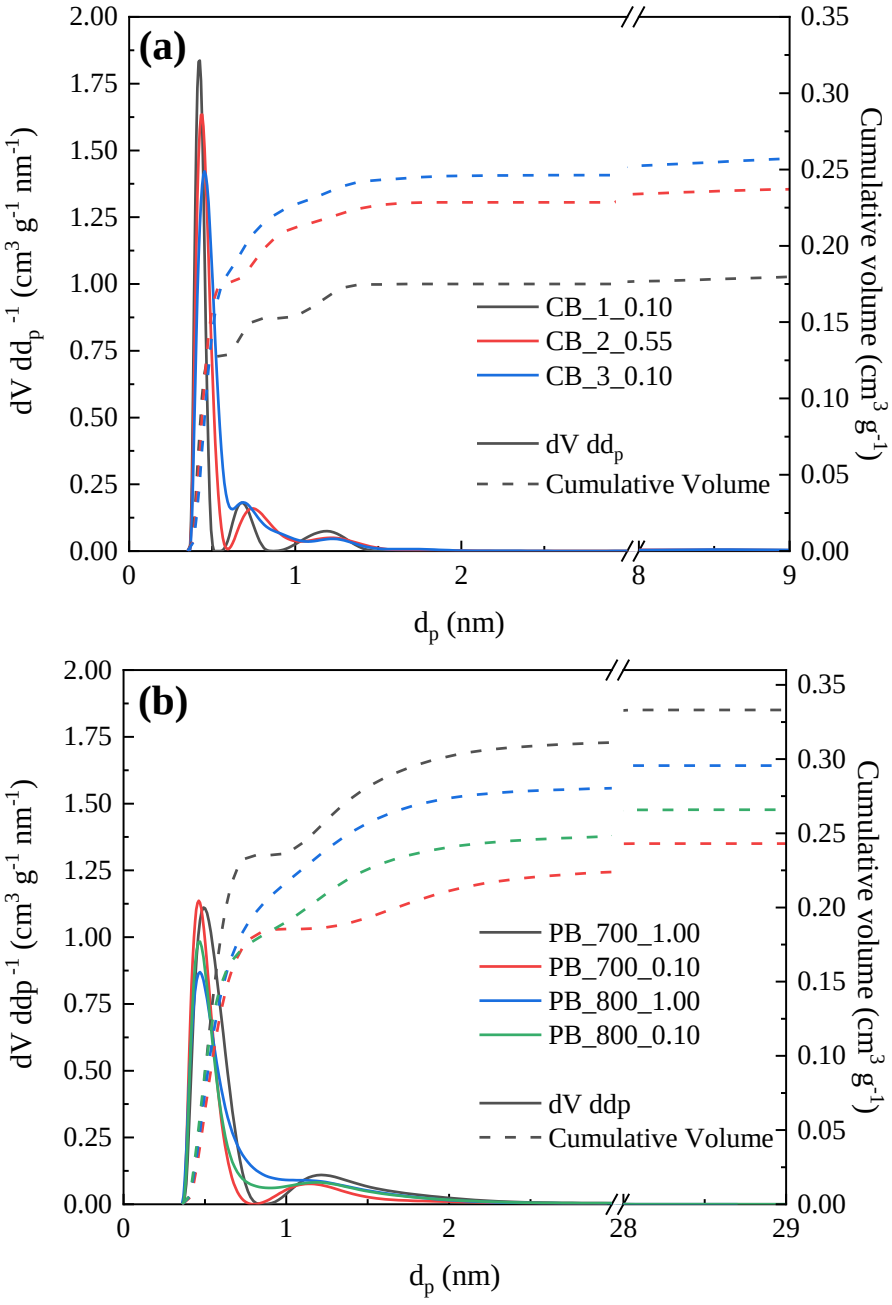

Fig. A.3. PSD and cumulative pore volume of chemical (a) and physical (b) activated biochars.

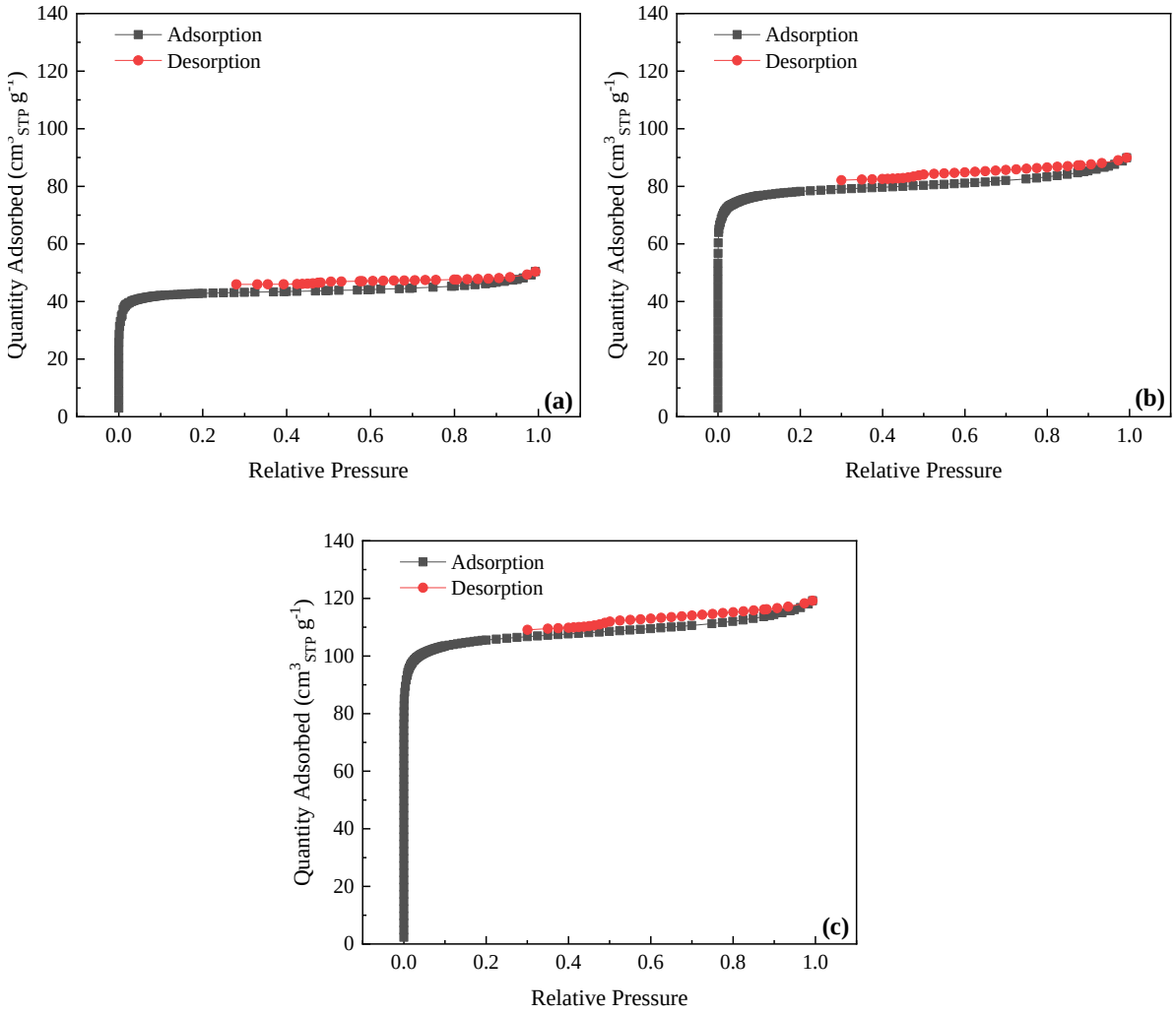

Fig. A.4. N_2 adsorption/desorption isotherms of the following chemically activated biochars: CB_3_0.10 (a); CB_2_0.55 (b); and CB_3_0.10 (c).

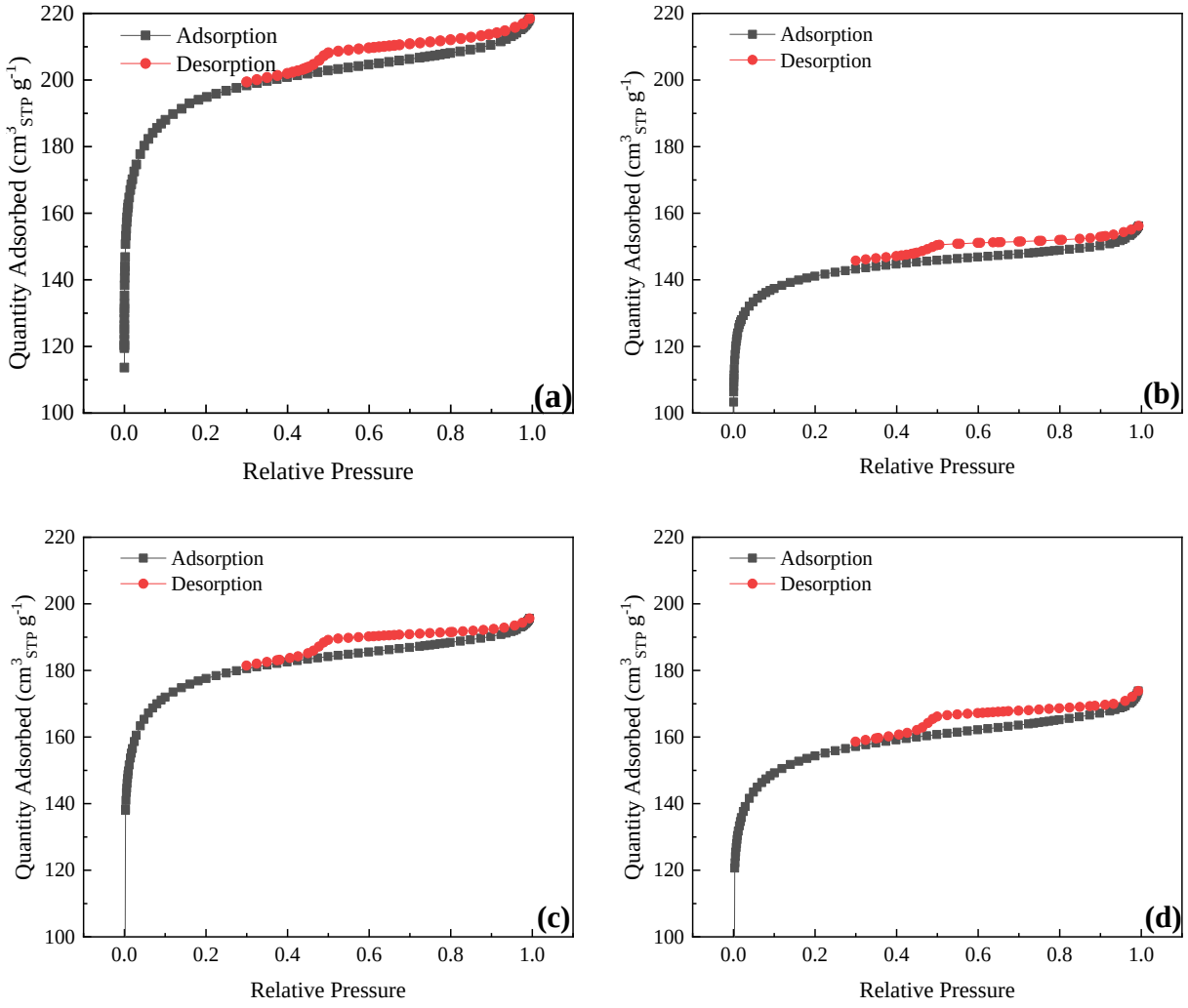

Fig. A.5. N_2 adsorption/desorption isotherms of the following physically activated biochars: PB_700_1.00 (a); PB_700_0.10 (b); PB_850_1.00 (c); and PB_850_0.10 (d).

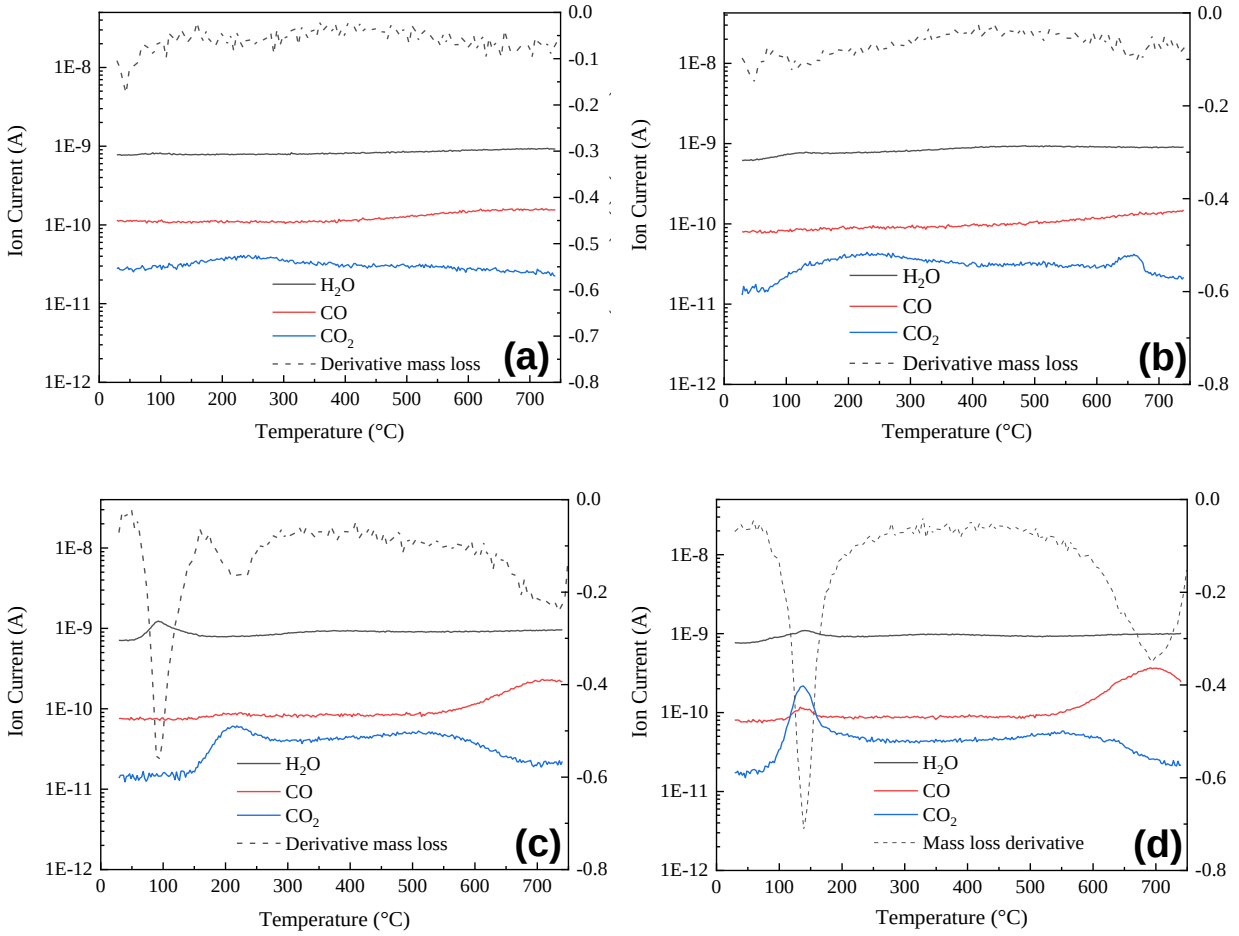

Fig. A.6. Differential thermogravimetric curves (in % of mass min^{-1}) and profiles of released species (H_2O, CO_2, and CO) from the TPD measurements conducted for the following materials: CB_3_0.10 (a); CB_3_0.10_W (b); CB_3_0.10_R (c); and PB_700_1.00+K_2CO_3 (d).

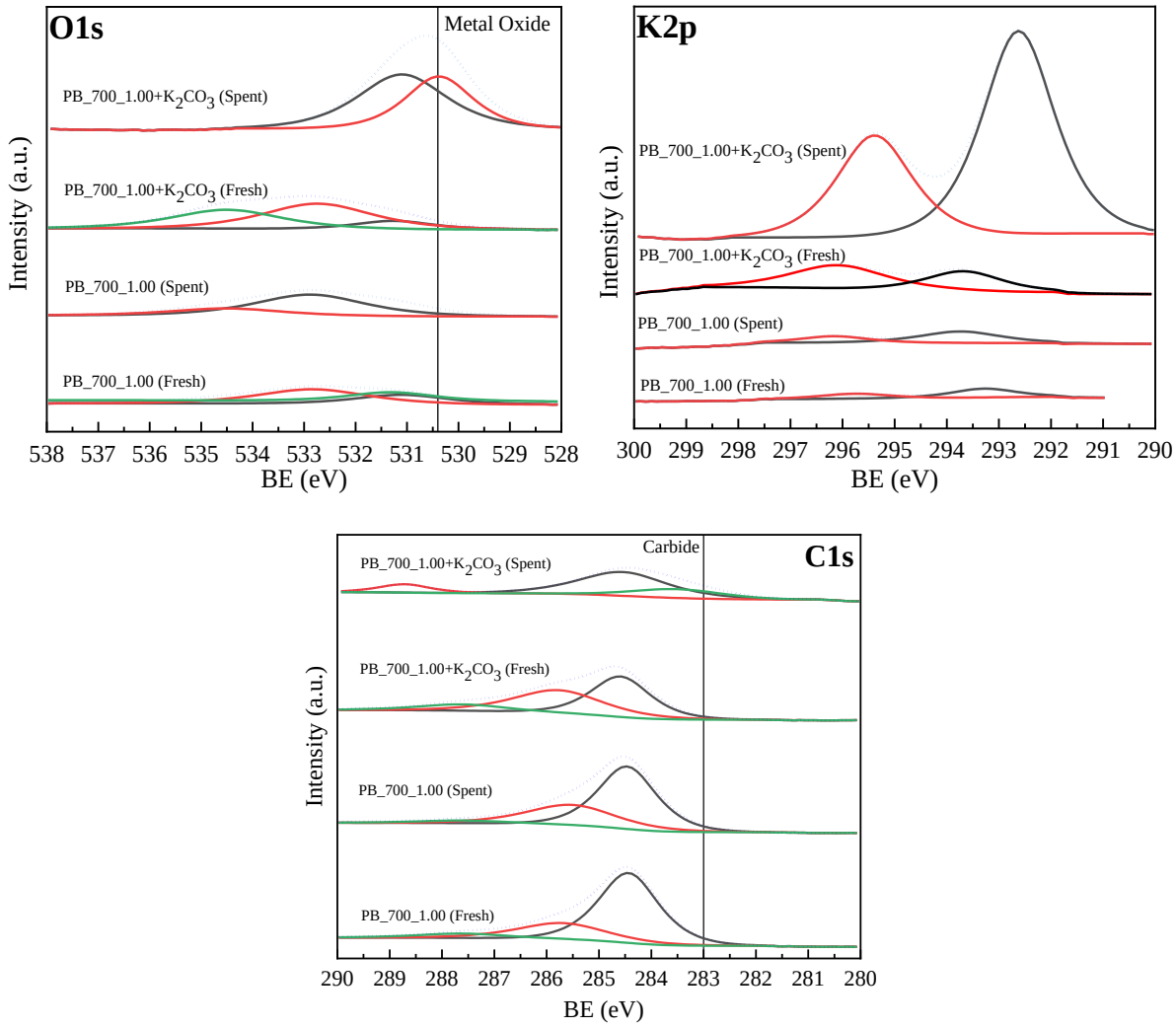

Fig. A.7. C1s, O1s and K2p spectra of fresh and spent PB_700_1.00 and PB_700_1.00+K_2CO_3.